GEOLOGY OF THE ICE COPPER-GOLD DEPOSIT, YUKON

Adam Fage
Supervisor: Dr. Marcos Zentilli

Submitted in Partial Fulfilment of the Requirements
For the Degree of Bachelor of Sciences, Honours
Department of Earth Sciences
Dalhousie University, Halifax, Nova Scotia
March 2008

DALHOUSIE UNIVERSITY
Inspiring Minds

Department of Earth Sciences
Halifax, Nova Scotia
Canada B3H 4J1
(902) 494-2358
FAX (902) 494-6889

DATE: April 24, 2008

AUTHOR: Adam Fage

TITLE: Geology of the Ice Copper-Gold Deposit, Vulcan

Degree: BSc (honours) Convocation: May Year: 2008

Permission is herewith granted to Dalhousie University to circulate and to have copied for non-commercial purposes, at its discretion, the above title upon the request of individuals or institutions.

Signature of Author

Table of Contents

List of Figures

ABSTRACT

The Ice copper-gold deposit is located in the Carmacks copper belt, UTM zone 08V, 417935E, 6905900N, Yukon. First staked in the early 1970s, it is currently being explored by BC Gold Corporation of Vancouver, British Columbia. Exploration has focused on the eastern edge of a bulls-eye positive aeromagnetic anomaly, measuring roughly 1000 m by 700 m. The Carmacks copper belt contains economic porphyry-type copper type deposits, such as the Minto and the Carmacks Copper. This study is based on field mapping, petrography, ore microscopy, microprobe analyses and rock geochemistry. It reviews exploration history in the context of genetic models and the known geology of other deposits in the region.

The Ice surficial rocks studied so far contain malachite and other copper oxides in pores and fractures, probably previously occupied by sulphides. Small irregular particles of native silver are present. Disseminated magnetite, partially oxidized to hematite (martite) accounts for the relatively high magnetic susceptibility of the rocks; however the association of copper with a magnetic anomaly seems to be fortuitous. The low-grade copper is hosted within variably sheared and altered hornblende-biotite granodiorite phases of the early Jurassic Granite Mountain Batholith. Fabrics and recrystallized quartz veinlets suggest that hydrothermal mineralization preceded deformation. It is suggested that, as previously established for the Minto and Carmacks Copper, the Ice deposit formed in the Jurassic at considerable depth (> 5 km) in a porphyry copper system, and that tectonic deformation (ductile shearing) followed the main mineralization event. Exhumation and extensive weathering occurred in the Cenozoic.

The positive correlation of copper values with potassium and rubidium is compatible with a primary association of copper with potassic alteration in a porphyry system; the occurrence of remnants of iron and native silver in vugs occupied by copper oxides suggests that these were occupied by hypogene minerals. The preferred model envisages a porphyry system sheared into a tabular foliated granodiorite body; structural mapping and radiometric surveys could be useful exploration tools. It is possible that some of the oxide mineralization has been displaced from its hypogene source by migrating groundwaters during the Cenozoic, making it an exotic (displaced, secondary) copper deposit.

Acknowledgments

I would like to thank BCGold Corp. and Brian Fowler for the opportunity to study this deposit; Shawn Ryan and Cathy Wood of Ryan-Wood Exploration for the great opportunity to work in the Yukon and for suggesting this project; Peter and Anne Ledwidge for instruction in the field.

Lexie Arnott for the help with geobarometry and geothermometry; Gordon Brown for preparing my thin and polished sections; Patricia Stoffyn for instruction on microprobe analyses; Patrick Ryall for guidance and suggestions on early drafts of the thesis; Keith Taylor for help with XRD analyses.

My family has given me a great deal of support throughout my undergraduate degree. Thank you Mom, Dad, Jill, Monique, Isaac, Cecille and Orion.

Finally, thank you to Dr. Marcos Zentilli, your countless hours of assistance made this project possible.

Financial assistance was given by BCGold Corporation and NSERC Discovery Grant No. 9036 to Dr. Marcos Zentilli.

Chapter 1

Introduction

1.1 General statement

The Ice copper-gold deposit is a prospect known since the early 1970s, situated in the Carmacks Copper Belt where two economic deposits are located. This thesis is a case study of the exploration activities at the Ice deposit, in which the author participated. This study includes field descriptions, petrography, analysis of available geochemical data, and evaluates various genetic models for the genesis of the Ice deposit. A comparison with the larger Minto and Williams Creek deposits allows the conclusion that the Ice deposit is potentially economic.

It is concluded that the deposit was formed either as a deformed porphyry copper type deposit or is an exotic copper deposit. Tectonic deformation, burial and exhumation appear to have followed the main mineralization event. Porphyry type deposits are large, low to medium grade deposits in which primary ore minerals are deposited within felsic to intermediate porphyritic intrusions (Eckstrand et al. 1995). Exotic deposits are secondary deposits that occur in paleodrainage networks leading away from primary porphyry deposits that have undergone supergene enrichment; during supergene enrichment, acid-oxidizing copper-bearing fluids escape the supergene enrichment system into the surrounding drainage network and flow downhill to sites where precipitation of copper oxides occurs (Mote et al. 2001).

1.2 Mineral deposits of the Carmacks Copper Belt

Figure 1.1 shows the location of the Ice property in the Yukon. The nature and origin of deposits in the Carmacks Copper Belt are poorly known because they are

deformed, metamorphosed, deeply weathered, variably oxidized and poorly exposed (Tafti and Mortenson, 2004). Figure 1.2 shows the two main deposits of the Carmacks Copper Belt as well as the Ice property superimposed on the regional geology.

Figure 1.1: Location map of the Ice property (and the Carmacks Copper Belt). The Ice is located at UTM zone 08V, 417935E, 6905900N.

1.2.1 Minto

The Minto project (Fig. 1.2), owned by the Sherwood Copper Corporation is located 240 km north of Whitehorse, Yukon Territory and 50 km northwest of the Ice property. The main zone of the Minto deposit contains measured and indicated resources

of about 8 million tones grading 1.89% Cu, 0.66 g/t Au and 7.7 g/t Ag (Dessureault et al. 2006). Copper is contained primarily in bornite and minor chalcopyrite.

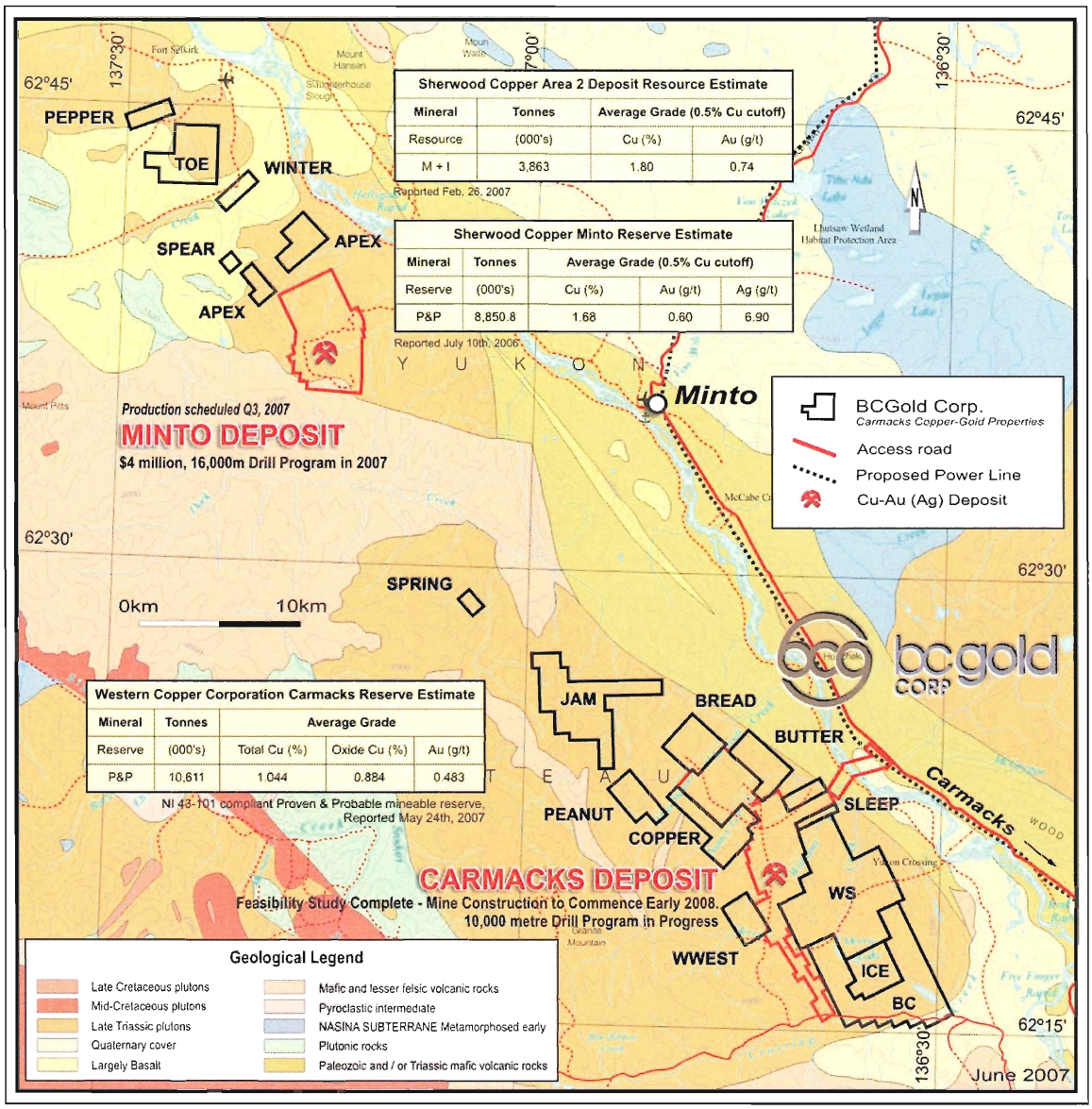

Figure 1.2: Location map of the Ice property on top of the regional geology. Also shown are the locations of the Minto and Williams Creek (Carmacks) deposits. (From http://www.bcgoldcorp.com/main/?carmacksmaps)

1.2.2 Williams Creek

The Williams Creek project (Fig 1.2), owned by Western Copper Corporation is located 200km north of Whitehorse, Yukon Territory, 40km southeast of the Minto

deposit and 10km northwest of the Ice property. The main zone of the Williams Creek deposit contains measured and indicated resources of about 10 million tones grading 1.044% Cu, 0.483 g/t Au, and 4.62 g/t Ag. (Robinson and Casselman, 2007)

1.3 Background of the Ice Property

The first report of copper in this region was made by Dr. G.M. Dawson (son of Sir William Dawson, after whom The Dawson Geology Club was named) in 1887 (Robinson and Casselman, 2007) concerning copper occurrences at Hoochekoo Bluff, located to the north of the property on the Yukon River. The first claims were staked in 1898 to cover copper showings that were associated with copper bearing quartz veins located in Williams Creek Canyon, 10km north of the property and Merrice Creek Canyon, 4 km north of the property.

In the spring of 2006, the Ice property was staked by Ryan-Wood Exploration Ltd. The property was named Ice after Merrice Lake (The last three letters of Merrice were taken), located 1.5km to the north of the property. In late 2006, the property was sold to BC Gold Corporation.

1.4 Questions to be answered

This thesis addressed some important questions such as:

- What are the Cu and Au bearing minerals in the Ice property?
- This area has not been glacially eroded; what implications does this have?
- What is the nature of hydrothermal alteration?
- Why is the mineralization associated with a positive magnetic anomaly?
- Was the mineralization pre- or post- regional deformation/metamorphism?

- Is the mineralization of porphyry copper type or something else?
- Are the Igneous Host rocks the same as at Minto and Williams Creek?
- Is the Ice at the same structural level/phase of the batholith as the other deposits?
- Was the Cu mineralization associated in any way with the magnetite; was the magnetite part of the ore suite or just a spatial coincidence?
- Is the oxidized copper replacing pre-existing sulphides in situ, or have the copper oxides been transported from elsewhere, making Ice an exotic deposit?

1.5 Objectives

1. To understand the correlation (or non-correlation) between magnetic anomalies and mineralization in the Ice area.
2. To determine the relative timing of mineralization and regional deformation/metamorphism.
3. A comparison of the mineralogy of alteration (feldspars and biotite)
4. To determine similarities/differences between the Ice and Minto/Williams Creek deposits.
5. To generate a genetic deposit model for the Ice deposit.

1.6 Methodology

In June 2007, geological mapping, trench mapping, geochemical sampling and rock sampling were done by the author under supervision of geologists Peter and Anne Ledwidge. Soil samples for ICP-MS (Inductively coupled plasma mass spectrometry) and MMI (Mobile Metal Ion) analysis were taken at 50 m station spacings trending north-

south along lines spaced 100 m apart. In September 2007, the rocks were photographed, described, and cut into slabs in the Department of Earth Sciences, Dalhousie University. Magnetic susceptibility of all of the rocks was measured. The slabs were photographed and thin sections made for petrography. Polished sections were created for ore petrography. Whole rock geochemical analyses, electron microprobe analyses, and X-ray diffraction identifications were done. Geochemical data were analyzed with statistical programs.

1.7 Organization of the Thesis

This thesis is divided into 8 chapters. Chapter 2 gives an overview of the regional geology around the study area. Chapter 3 gives an overview of the history of the Ice property, as well as the geophysics, geochemistry, and the field geology of the property. Chapter 4 describes the field work done at the Ice property, as well as the stratigraphy and structural geology of the area. Chapter 5 deals with the igneous petrology of the Ice property. Chapter 6 deals with the mineralogy of alteration and ores at the Ice property. Chapter 7 gives a genetic model for the Ice property. Chapter 8 presents the conclusion of the thesis and recommendations for future work. Appendices follow that contain sample descriptions, microprobe data, geochemical data, and methodologies.

Chapter 2

Regional Geology

2.1 Tectonic Framework

The Carmacks Copper Belt lies within the Yukon-Tanana Terrane of western Canada. The metamorphic rocks in central-eastern Yukon and central western Alaska have also been described as being part of the Yukon Crystalline Terrane by Tempelman-Kluit (1976).

Tafti and Mortenson (2004) concluded that the Minto and Williams Creek deposits formed during a major period of 'vertical tectonics' that affected the region. Regional-scale uplift from mid-crustal to shallow depths at ~186 Ma was deduced from field and U-Pb dating studies of the Aishihik batholith and Lang Lake plutonic suite intrusions 70km to the southwest (Tafti and Mortenson, 2004). There is also evidence for crustal scale thickening throughout large portions of the Yukon-Tanana terrane in western Yukon and eastern Alaska between ~195 to 185 Ma, which could coincide with the burial of the mineralizing systems at Minto and Williams creek (Tafti and Mortenson, 2004). The crustal thickening, burial, and uplift of the region must have occurred within an active continental arc setting, since Tafti and Mortenson (2004) recognized that the geochemical signature of the intrusives is indicative of a continental magmatic arc.

2.2 Stratigraphy

The porphyritic granodiorite is ascribed into the Granite Mountain batholith, interpreted to be intruded into the Yukon- Tanana Terrane. The batholithic rocks are in fault with, or intruded into an unnamed package of altered mafic volcanic rocks to the

northeast and are unconformably overlain by sedimentary rocks and volcanics of the Late Cretaceous Tantalus Formation and Late Cretaceous Carmacks Group, respectively (Tafti and Mortenson, 2004).

2.3 Structural Geology

Tafti and Mortenson (2004) have described the structural geology of the area, although the regional structure is poorly understood because outcrop is very sparse (<1%) and the area is unglaciated and deeply weathered. They found that generalized alignment of K-feldspar phenocrysts in the porphyritic granodiorite indicate magmatic flow. Post-mineralization deformation includes brittle faults with several orientations, including the DEF fault which forms the northern boundary of the main zone at Minto (Tafti and Mortenson, 2004). There is also evidence of block rotation, evidenced by the tilting of younger sedimentary units. This block rotation may account for anomalously shallow dips of the dominant foliations in gneissic host rocks at Minto (Tafti and Mortenson, 2004).

2.4 Igneous History

The rocks of the Ice property are entirely made up of granodiorites of the Granite Mountain Batholith which has been dated by Tafti and Mortenson (2004) to be Early Jurassic (~194 Ma). Post-mineralization granite pegmatite and aplite dykes are widespread in the area. The Ice rocks are plotted on a QAP (Quartz-Alkali Feldspar-Plagioclase) diagram in figure 2.1.

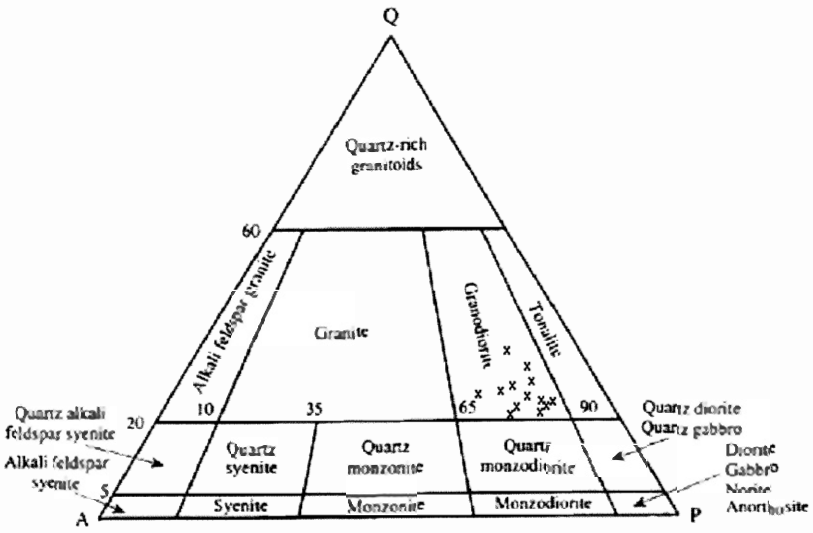

Figure 2.1: Plutonic rocks from the Ice property plotted onto a QAP diagram, from petrographic analysis by the author.

2.5 Metamorphic History

The area has not undergone regional metamorphism, but rafts of host rock within the granodiorite body are locally contact metamorphosed. There are no metamorphic rocks at the Ice property, but Tafti and Mortenson (2004) have described amphibolite/biotite-schist as xenoliths at Williams Creek.

2.6 Metallogeny

At Minto and Williams Creek, the main host rocks for the deposits are variably deformed plutonic rocks. The following description is based on Tafti and Mortenson (2004). Mineralization at Minto is hosted within foliated biotite and quartzofeldspathic orthogneiss, with a lesser amount contained within a banded, relatively quartz-rich rock. The ore zones are enclosed within massive to weakly foliated granodiorite. The host rock for the Williams Creek deposit is foliated intrusive rock of dioritic to quartz dioritic composition, also enclosed within massive to weakly foliated granodiorite. At both

deposits, chalcopyrite, bornite and lesser pyrite are disseminated and occur as stringers (Tafti and Mortenson, 2004).

At the Ice property, mineralization has only been observed as malachite in weakly to strongly foliated granodiorite. Mineralization is interpreted to have occurred prior to the pervasive structural deformation that has affected the host units. No primary sulfide minerals were encountered.

2.7 Geomorphology

Tempelman-Kluit (1980) has given a good synthesis of the evolution of the physiography and paleodrainage of the southern Yukon from the Miocene to present. Before the rapid rise of the St. Elias Mountains, uplift of the Pelly Range and other ranges in southern Yukon and the formation of the Tintina Trench in the Pliocene, southern Yukon had comparatively low relief. The southwestern barrier of the St. Elias Mountains (Fig 2.3) did not exist at this time, which may have allowed water to drain directly to the Pacific via a now abandoned southwesterly route. This deserted drainage hypothesis can explain inconsistencies in relative maturity of parts of valleys, for example, the Takhini and Dezadeash Rivers are small for the valley that they occupy; this valley is considered to be the outlet to the coast of the abandoned drainage. The Yukon River valley in the area of the Klondike is small for its present stream, and the White Channel Gravels and equivalents from the old alluvial surface slope to the southeast in this area, opposite to the gradient of present streams. Figure 2.2 shows the hypothetical paleodrainage as well as the current drainage (Tempelman-Kluit, 1980).

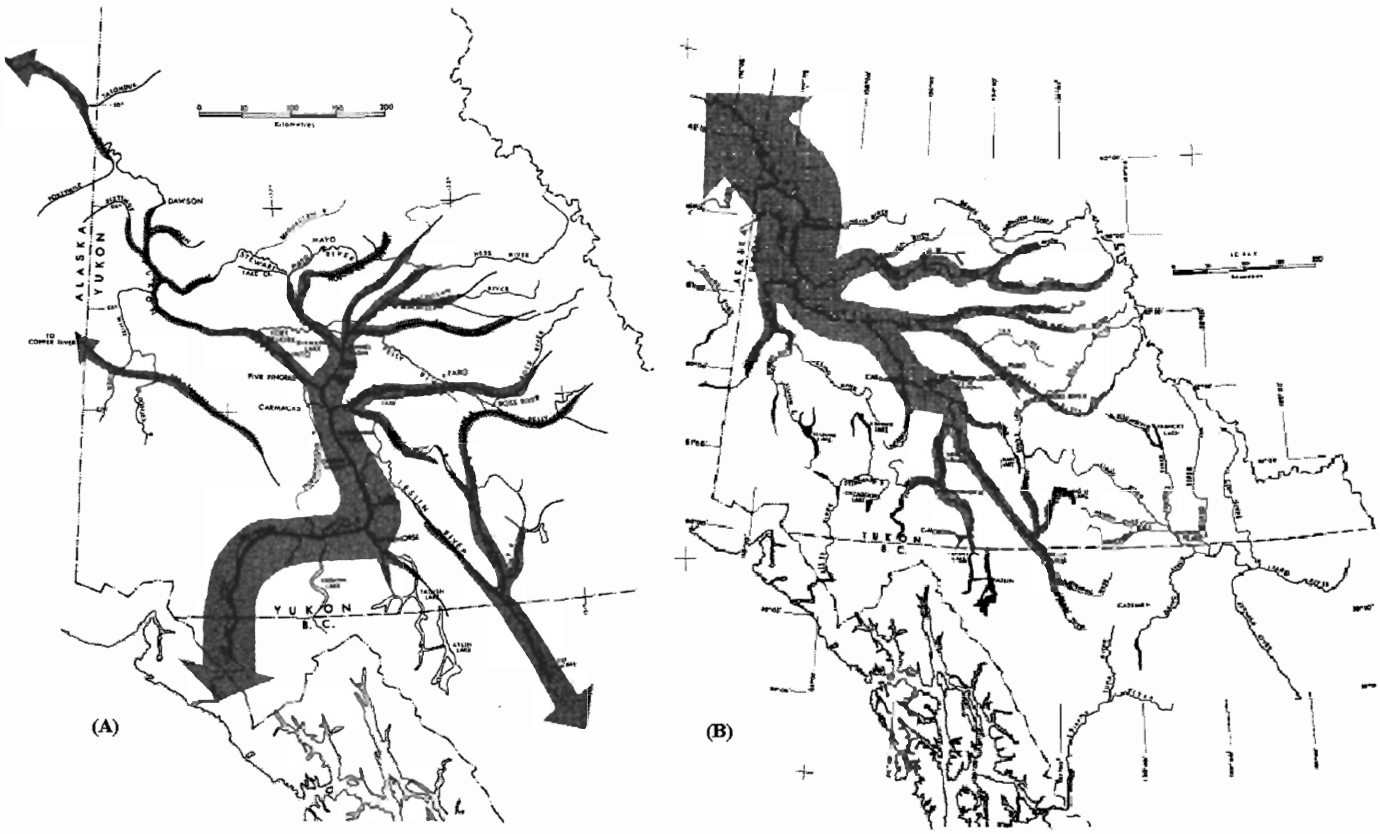

Figure 2.2: A) Hypothetical southwest-flowing drainage (gray arrows) of southern Yukon that probably existed during the Miocene and Pliocene. Water probably drained directly to the Pacific through the valley of the Takhini-Dezadeash Rivers via the ancestral Stikine River. B) The modern, northwest-flowing drainage is shown for comparison. (After Tempelman-Kluit, 1980)

Rerouting of the direct southwesterly drainage to the present northwesterly course probably occurred during the Pleistocene due to damming by glacial Ice in the St. Elias Mountains. When deglaciation began, ice melted in the interior but remained in the St. Elias Mountains preventing drainage to the coast via the old route and initiating rerouting of the drainage to its present route (Tempelman-Kluit, 1980).

The newer drainage is a long and circuitous route in comparison to the old route; for example, Lake Laberge, near Whitehorse, at about 600m above sea level drains to the Pacific through about 2500km of Yukon River, while along the Takhini-Dezadeash route the distance to the Pacific is only 300km (Tempelman-Kluit, 1980).

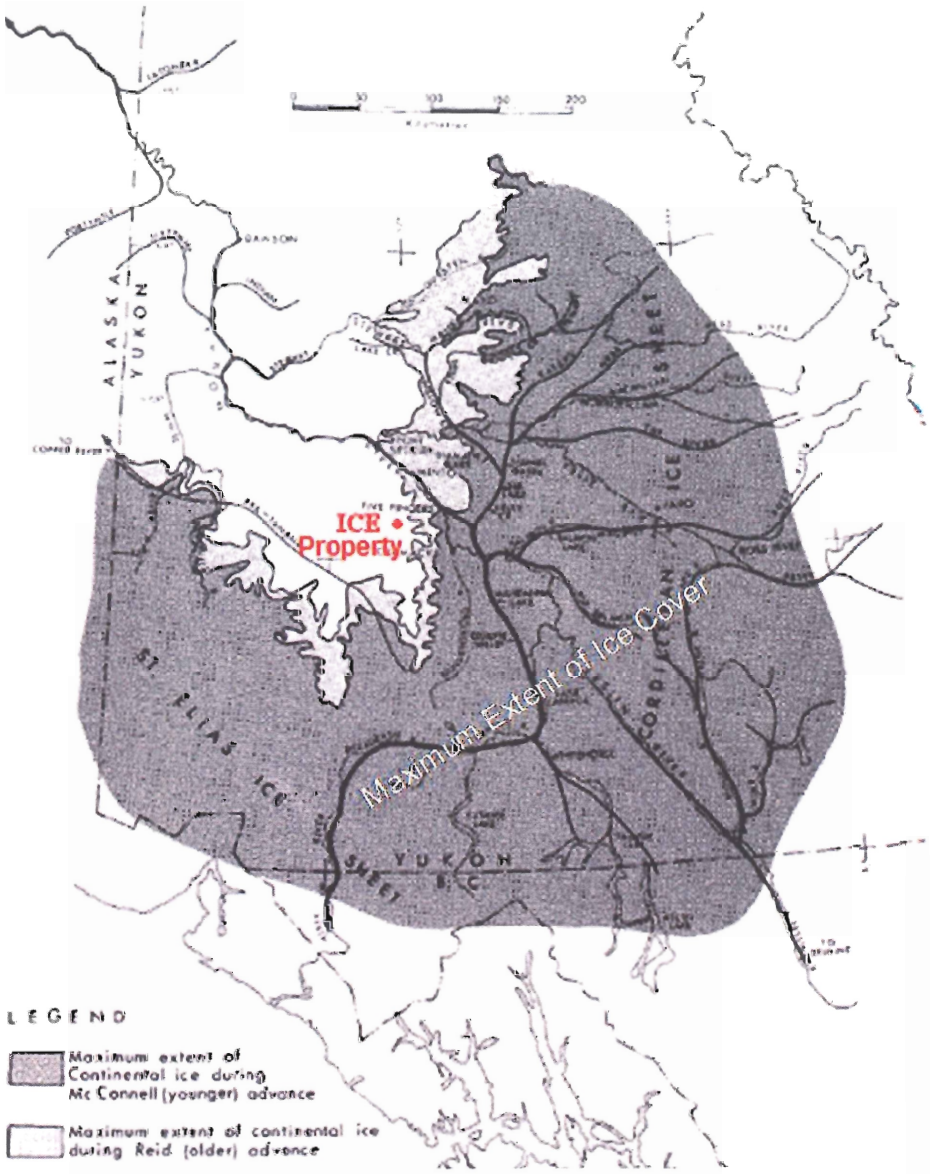

Figure 2.3: Extent of continental ice during the two latest glacial advances of the Pleistocene. Hypothetical Drainage is shown on top of current drainage for reference. The St. Elias Mountains are located in south-western Yukon in the area of the St. Elias Ice Sheet. Darker areas denote glaciation (After Tempelman-Kluit, 1980).

Figure 2.3 shows the extent of continental ice during the two latest advances of continental ice sheets during the Pleistocene. If the deeply weathered rocks of the Ice property had been affected by a glaciation, they would have been easily broken up and transported away by the continental ice sheet, probably removing any evidence of the deposit.

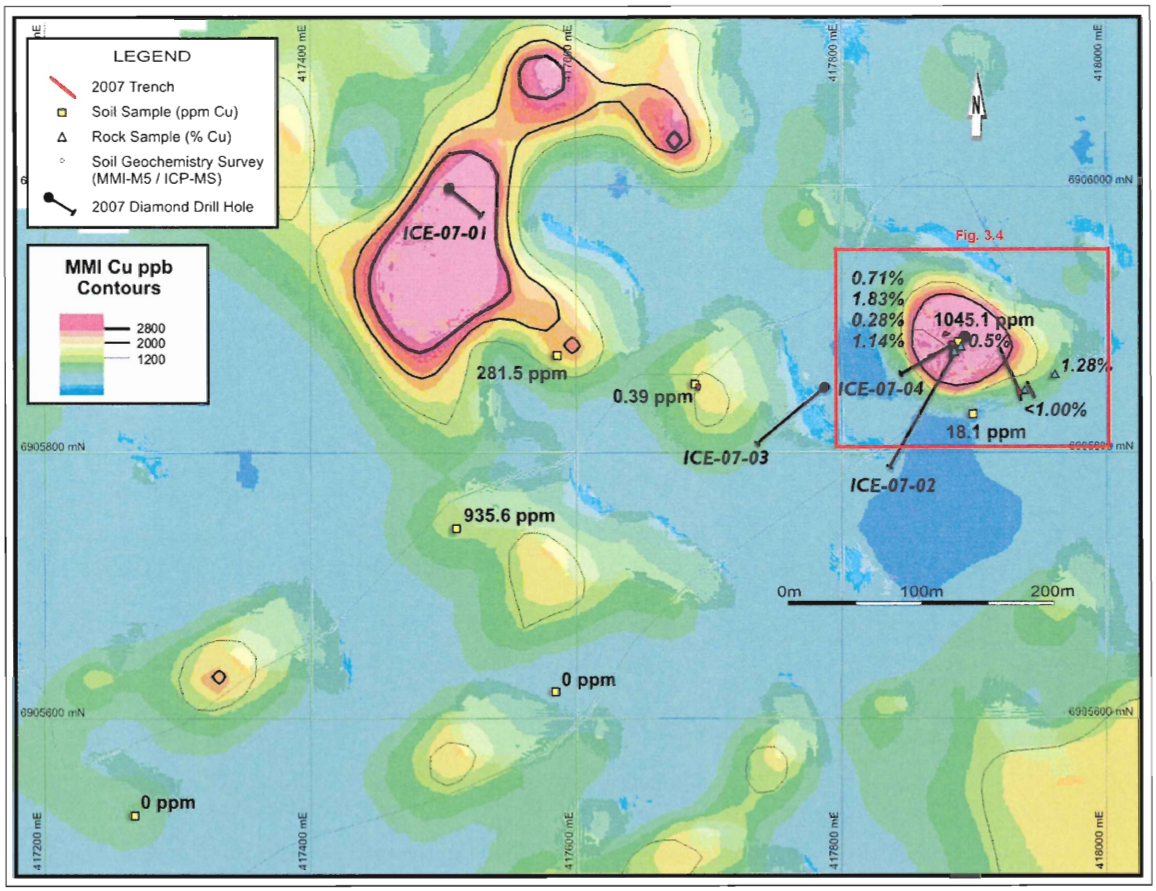

Figure 3.3: Copper MMI contours at the Ice zone. Locations of 2007 diamond drill holes are also indicated. (After http://www.bcgoldcorp.com/main/?carmacksmaps)

A geochemical study by Tafti and Mortenson (2004) indicates that most intrusive rocks in the adjacent Williams Creek deposit are subalkaline, and weakly to moderately peraluminous. Concentrations of immobile trace, high field-strength and rare-earth elements are consistent with generation in a continental magmatic arc and indicate that intrusive rocks in this area are geochemically very similar to other Late Triassic and Early Jurassic intrusive rocks elsewhere in the Yukon-Tanana Terrane in Yukon and eastern Alaska as described by Mortensen et al. (2000) and Tafti and Mortenson, (2004).

3.4 Field Geology

The rocks at the Ice and Williams South properties consist of intermediate to felsic intrusive and meta-intrusive rocks of the early Mesozoic Granite Mountain Batholith. The area is unglaciated and deeply weathered, outcrop is very sparse (<1%), and regional structure is poorly understood. The area is overlain by 1-5cm of volcanic ash from a distal source. The rocks at the Ice zone range from foliated biotite granodiorite to biotite +/- hornblende granodiorite to hornblende granodiorite. The rocks also range from non-magnetic to strongly magnetic. Felsic aplite dykes ranging from 1-40cm in thickness are present as well as pegmatitic dykes ranging from 1-20cm in thickness. Rocks that contain malachite mineralization contain biotite and are also weakly to strongly foliated. Figure 3.4 shows the detailed geology of the Ice property.

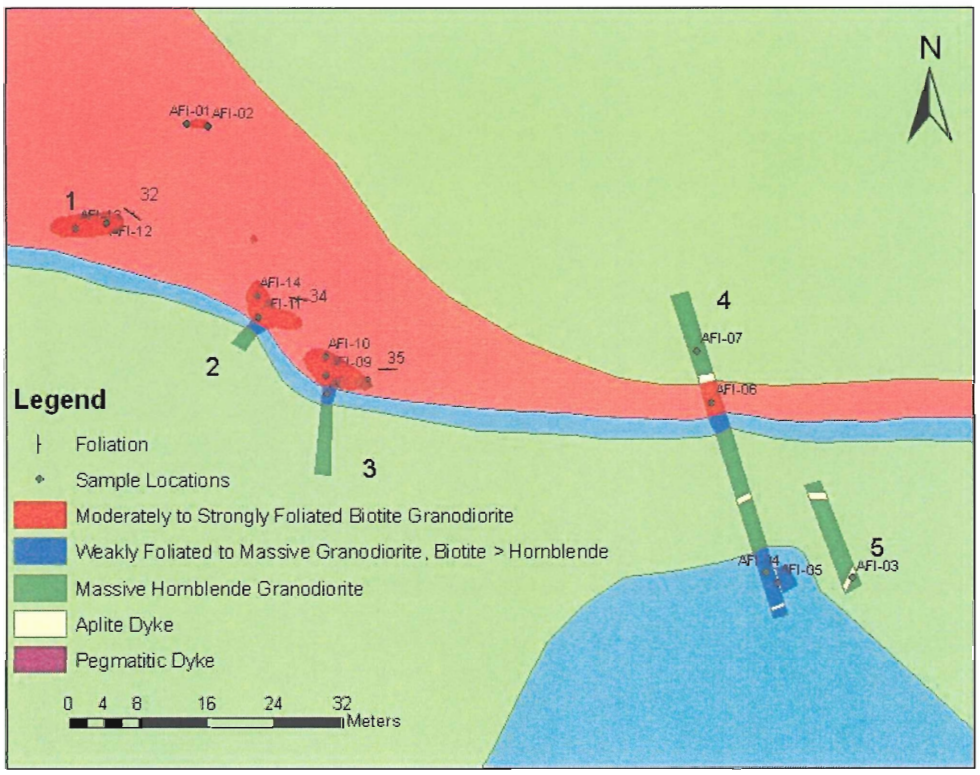

Figure 3.4: Detailed geology of the outcrops and five trenches of the Ice property. Darker colours denote outcrop and trenches; lighter colors are inferred bedrock geology. Copper mineralization is found primarily in the moderately to strongly foliated biotite granodiorite unit.

Chapter 4

Geology of the Ice Property

4.1 Field Work

In June 2007, the author participated in a regional mapping project of the properties surrounding the Ice, and created a detailed map of the outcrops and trenches at the mineralized zone of the Ice property. 14 Rock samples collected by the author were grab samples selected to study differences in mineralogy in both mineralized and unmineralized phases of the granodiorite. Five trenches were dug over an aera approximately 100mx75m on top and down the southwest side of a hill (Fig. 3.4) to increase bedrock exposure, as exposure is sparse in the area (<1%), using a lightweight backhoe which could be transported to the site via helicopter. Structural measurements are reported using the right hand rule.

Trench #1, dug next to mineralized subcrop, is approximately 8m x 2m, and is entirely composed of magnetic, mineralized (1-3% malachite), weakly foliated biotite granodiorite. Trench #1 has a foliation of 306/32 NE and contains a 2-5 cm thick pegmatite dyke with a strike of 240/65 N. About 10m to the north of trench #1, there is subcrop of weakly magnetic, foliated, mineralized biotite granodiorite.

Trench #2 was dug at the base of a 5 m^2 outcrop of magnetic, mineralized (1-3% malachite), foliated biotite granodiorite with a foliation of 276/34 N. Trench #2 is approximately 5m long and 1m wide, at the base of the outcrop there is a sharp contact between the magnetic, mineralized, foliated biotite granodiorite and massive, weakly magnetic biotite granodiorite which grades into massive hornblende granodiorite over 1m past the contact into the trench.

Figure 5.1: Outcrop at the top of trench #3 at the Ice property. A clear contact is visible between foliated, mineralized granodiorite (upper) and massive unmineralized granodiorite (lower). Sample AFI-14 was taken from the foliated section of this outcrop.

Figure 5.2: Hand specimen of sample AFI-14A. Copper oxide is visible in the rock as well as rusty vugs (scale bar is in cm).

5.2 Microscopic Igneous Petrography

Thin sections were prepared for 12 samples and polished sections were prepared for 10 samples at Dalhousie University in the fall of 2007. Thin section descriptions are given in Appendix 1. Polished sections were analyzed with the electron microprobe at Dalhousie University's Robert Mackay Laboratory. Figure 5.3 shows a grain of magnetite partially oxidized to hematite (martite). The rocks at the Ice property are heavily weathered and oxidized.

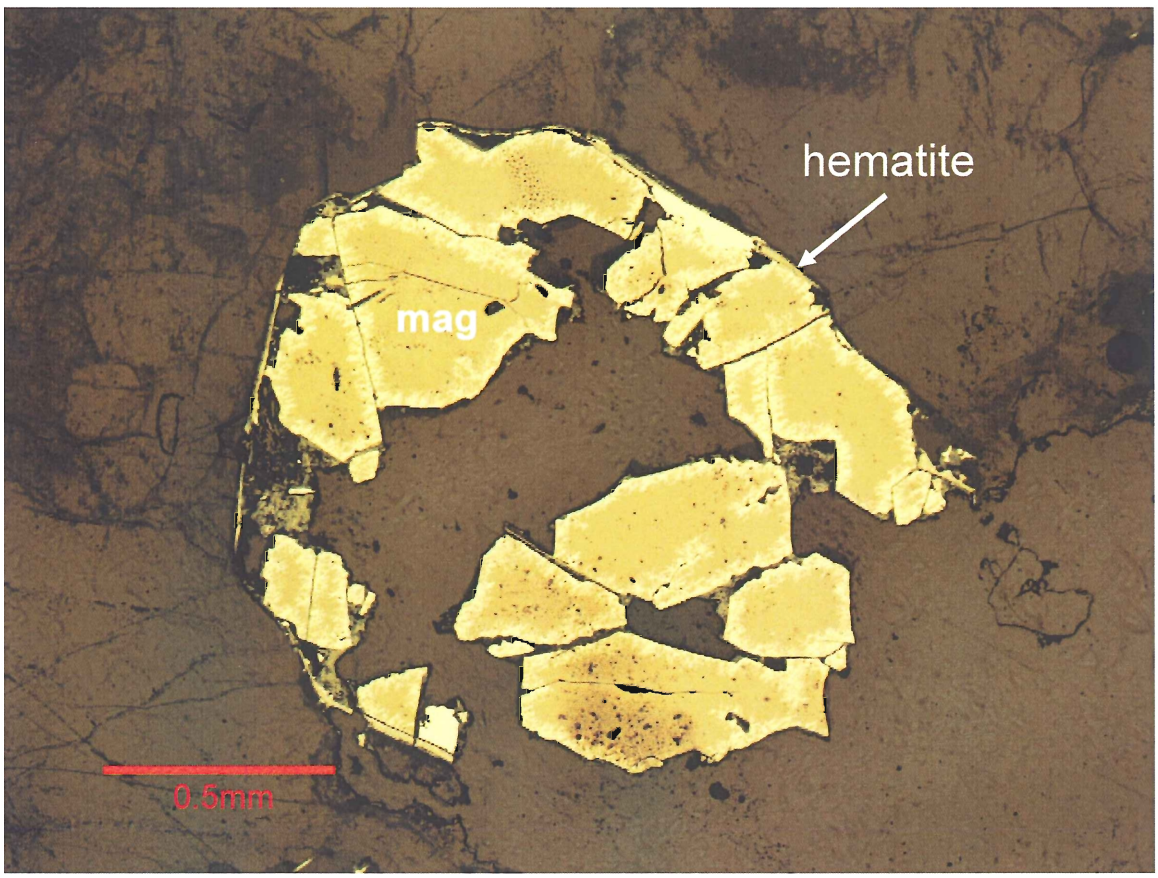

Figure 5.3: Polished section picture (Sample AFI-14b) showing a magnetite grain partially oxidized to hematite (martite).

The foliation of the foliated granodiorite is defined by grains of biotite; figure 5.4 shows biotite grains defining a foliation in sample AFI-13.

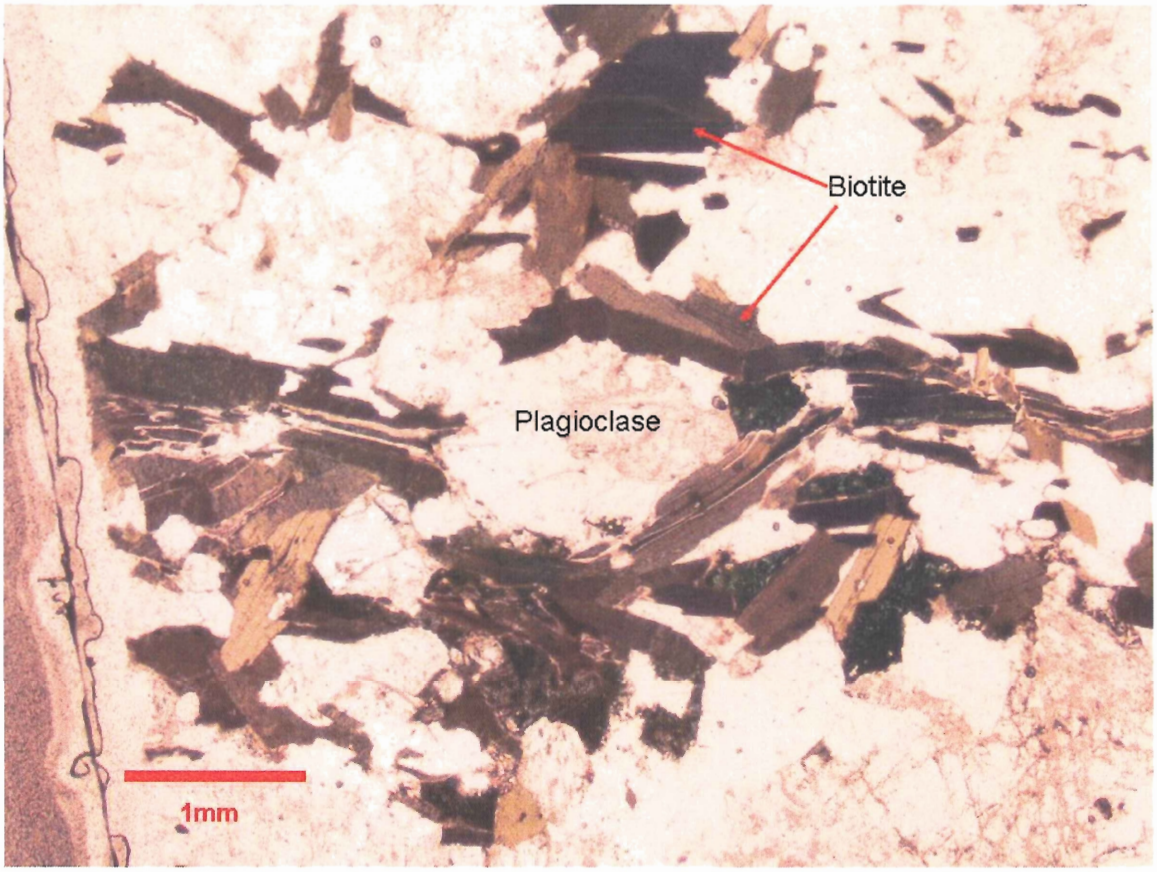

Figure 5.4: Biotite grains defining a foliation in sample AFI-13. The foliation is a secondary feature related to tectonic deformation and wraps around a plagioclase grain.

Recrystallized quartz veinlets are visible in thin section which indicates that the rocks have undergone tectonic strain.

5.3 Geochemistry

Ten samples were analyzed by Geo Labs in Sudbury, ON for whole-rock major and trace elements and ferrous iron (FeO) using X-ray fluorescence spectrometry (XRF). Appendix 3 shows these analyses. FeO analyses have not yet been returned by the lab (March 11, 2008).

Increased copper values correlate with an increase in As, Sn, Rb, Pb, Ba, and K_2O and a decrease in Na_2O, and LOI (Loss on ignition).

A plot of Nb vs. Y and a plot of Rb versus Y+Nb (Fig 5.5) indicates a volcanic arc setting for the intrusive rocks of the Ice property (Pearce et al., 1984) which agrees with Tafti and Mortenson's (2004) findings.

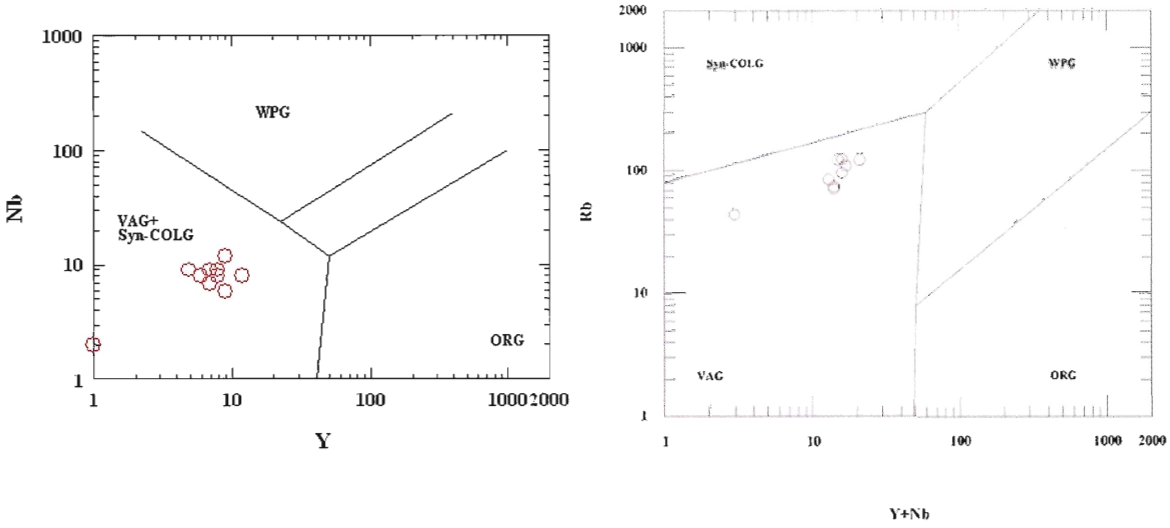

Figure 5.5: A logarithmic plot of Nb vs. Y indicates that the Ice granodiorites were formed within a syn-collisional or volcanic arc setting; a logarithmic plot of Rb vs Y+Nb for the Ice indicates that the igneous rocks formed in a volcanic arc setting (VAG = Volcanic Arc Granite, Syn-ColG = Syn-Collisional Granite). (After Pearce and Cann, 1973).

Figure 5.6 shows the Ice rocks classified based on geochemical data.

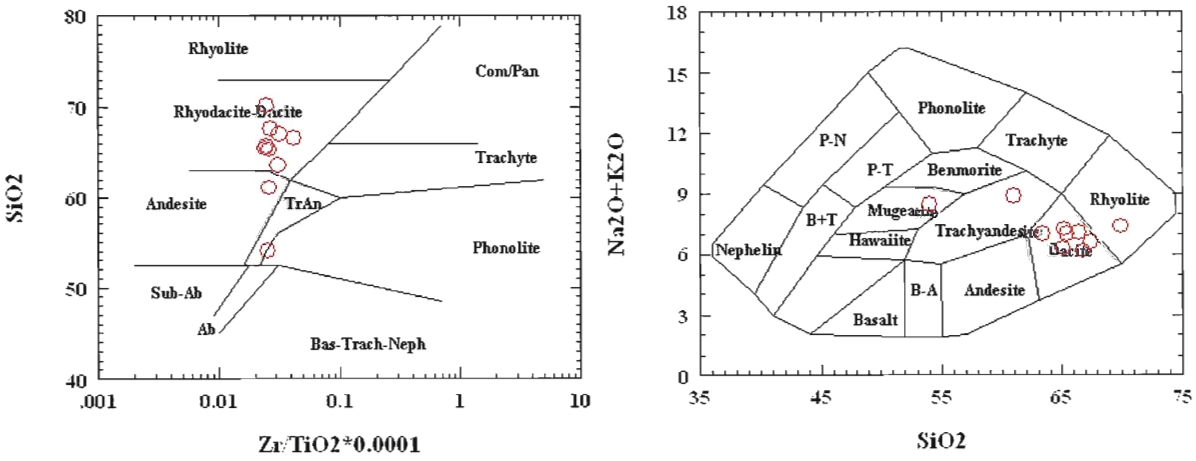

Figure 5.6: Two different rock classification diagrams illustrating that the rocks from the Ice property primarily fall under the granodiorite category (Dacite is the volcanic equivalent of Granodiorite). (After Winchester and Floyd, 1977).

A plot of logCu vs. K_2O indicates that higher copper values correspond to increased levels of potassium in the rocks, which is most probably due to potassic alteration, rather than a different intrusive body. Rubidium often substitutes for potassium, and a plot of logCu vs. Rb also shows a positive correlation which helps to validate this observation. These plots are shown in figure 5.7.

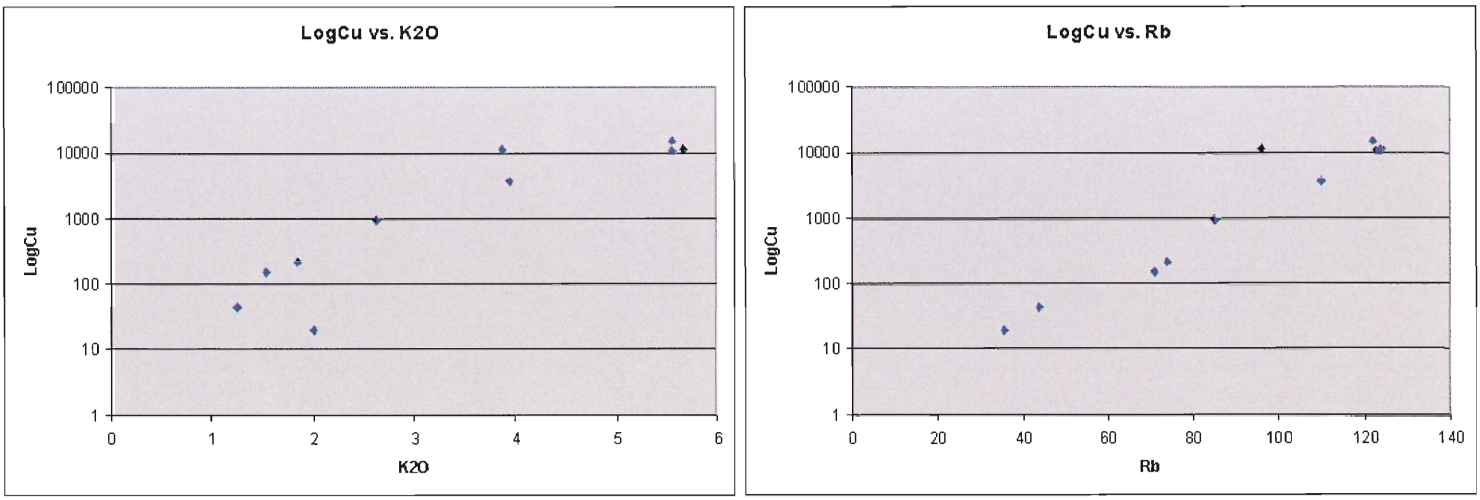

Figure 5.7: Plots of logCu vs. K_2O and logCu vs. Rb show a positive correlation which suggests that high copper values correspond to potassic alteration of the igneous rocks in a porphyry copper setting.

5.4 Hornblende Geobarometry and Two-Feldspar Geothermometry

The amphiboles used in this experiment have been classified as magnesian hastingsitic hornblende using Hawthorne (1981)'s classification system.

There are enough thermodynamic constraints on the composition of hornblende that the total aluminum values in the rims of hornblende of calc-alkaline rocks may be used to calculate the pressure of crystallization (Hammarstrom and Zen, 1986; Hollister et al. 1987; Schmidt, 1992). The requirements to constrain the degrees of freedom and make the Al-content of hornblende a valid geobarometer are the following (Hammarstrom and Zen, 1986; Hollister et al. 1987):

1) The rocks should be calc-alkaline;

2) An assemblage of plagioclase-quartz-hornblende-biotite-orthoclase-magnetite-titanite must have crystallized together;

3) To constrain temperature, only the compositions of the rims of the hornblende should be determined (the rims were the only part of the grains that could have crystallized with the other phases in the final melt);

4) The plagioclase rim compositions should be between An_{25} and $An_{35;}$

5) The pressure has to have been >2 kbars (the limit of the experiment).

Schmidt (1992) gives the following equation to calculate the pressure:

$$P\ (\pm\ 0.6\ \text{kbar}) = -3.01 + 4.76Al^{tot} \qquad (5.1)$$

Where P is the pressure in kilobars and Al^{tot} is the total aluminum in the hornblende in apfu (atoms per formula unit). Microprobe data for hornblendes are found in appendix 4b. The values for mass percent of aluminum range from 10.652 to 11.983 with a mean of 11.423. The apfu for all elements were calculated for all microprobe analyses and were found to be very similar. Table 5.1 shows the data for analysis AFI-07-32 calculated to apfu, assuming that all of the Fe is ferric.

Using Schmidt (1992)'s equation a value of 6.40 kbar is found for the pressure of solidification of this hornblende.

Oxygens per formula =		23.000						
Oxide	**GFW**	**FeO only Wt.%**	**Fe2O3 only Wt.%**	**Mole Units**	**Oxygen Units**	**Normaliz. Ox Units**	**Atom Units**	
SiO2	60.084	40.9131	40.913	0.681	1.362	12.000	6.000	**Si**
TiO2	79.866	0.8727	0.873	0.011	0.022	0.193	0.096	**Ti**
Al2O3	101.961	11.4373	11.437	0.112	0.337	2.965	1.977	**Al**
Fe2O3	159.688		21.967	0.138	0.413	3.637	2.424	**Fe+3**
FeO	71.844	19.7662					0.000	**Fe+2**
MnO	70.937	0.6631	0.663	0.009	0.009	0.082	0.082	**Mn**
MgO	40.304	8.8618	8.862	0.220	0.220	1.937	1.937	**Mg**
CaO	56.077	11.6663	11.666	0.208	0.208	1.833	1.833	**Ca**
Na2O	61.979	1.5049	1.505	0.024	0.024	0.214	0.428	**Na**
K2O	94.196	1.4774	1.477	0.016	0.016	0.138	0.276	**K**
H2O	18.015						2.000	**H**
Totals		97.2173	99.364	1.419	2.610	23.000	17.055	

Table 5.1: Microprobe analysis AFI-07-32 of a hornblende used in hornblende geobarometry calculations. This analysis was chosen as it has median numbers in all elements (Table after Leake et al., 1997).

The following equation is a two-feldspar geothermometer as given by Haselton et al. (1983):

$$T_K = \frac{(X^{AF}_{Or})^2(18810+17030X^{AF}_{Ab}+0.364P) - (X^{Pl}_{An})^2(28230-39520X^{Pl}_{Ab})}{10.3(X^{AF}_{Or})^2+8.3143\ln\left\{\frac{(X^{Pl}_{Ab})^2(2-X^{Pl}_{Ab})}{X^{AF}_{Ab}}\right\}} \quad (5.3)$$

Where T_K is temperature in degrees Kelvin, X= the mole fraction for the feldspars and P is the pressure in bars. No error is given for this calculation.

Using the pressure from equation 5.1 and the average feldspar values of Or_{82} and An_{30}, a value of 657°C is calculated (the increase in pressure to account for temperature

used in the following paragraph increased the calculated temperature to 660°C which is a negligible increase).

Anderson and Smith (1995) have added to the hornblende geobarometry equation to account for the effects of temperature on the Al-in-hornblende geobarometer; the revised equation is:

$$P\ (\pm\ 0.6\ kbar) = 4.76Al^{tot}\text{-}3.01\text{-}[(T\text{-}675)/85)]\ [0.530Al^{tot} + 0.005294(T\text{-}675)] \quad (5.2)$$

Where P is the pressure in kilobars, Al^{tot} is the total aluminum in the hornblende in apfu (atoms per formula unit) and T is temperature in °C. Using the temperature value calculated in the next section, the pressure of solidification for this hornblende is calculated to be 6.60 kbar.

5.5 Interpretations

The foliation observed in hand sample and thin section scales is a secondary feature related to tectonic deformation. Potassic alteration correlates to higher copper grades, and the foliation defining the higher grade areas are defined by biotite. The geochemistry of the Ice rocks indicates that they are granodiorites formed in a volcanic arc setting.

Using the Al-in-hornblende geobarometer, Tafti and Mortenson (2004) have found that the latest intrusive phases at Minto and Williams Creek formed at depths greater than 9km and have given a value of <6 kbar. Using amphibole-plagioclase thermometry, they have calculated the crystallization temperature at 720°C to 840°C which is low for intrusive rocks with granodioritic to dioritic composition (Tafti and Mortenson, 2004).

The Al-in-hornblende geobarometry values of 6.4-6.6 ±0.6 kbar correlate to depths of 18-20km and agree with Tafti and Mortenson (2003)'s findings. The calculated crystallization temperature of about 660°C is lower than Tafti and Mortenson's, but with the amount of error involved in geothermometry calculations, they may actually be in the same range.

The geobarometric calculations are tentative, and completed mainly to compare with similar work by other authors. The rocks at Ice do not qualify as calc-alkaline, but nor did those used by Tafti and Mortenson (2003). Also, without determination of the valency state of the Fe in the hornblende, which is out of the scope of this study, the uncertainty of the pressure calculation is considerable. Nevertheless, the results are consistent with crystallization of the rocks at several kilometres depth, such as is considered common for porphyry copper type systems (e.g. Lowell and Guilbert, 1970).

Chapter 6

Mineralogy of Alteration and Ores

6.1 Thin section descriptions

Thin section descriptions are in Appendix 1. From thin section analysis, the rocks were confirmed to be granodiorite. Strong foliations are visible in some samples, as well as recrystallised quartz, plagioclase and alkali feldspar grains. Foliated granodiorite from sample AFI-05, foliation defined by biotite, with a carbonate rim is shown in figure 6.1.

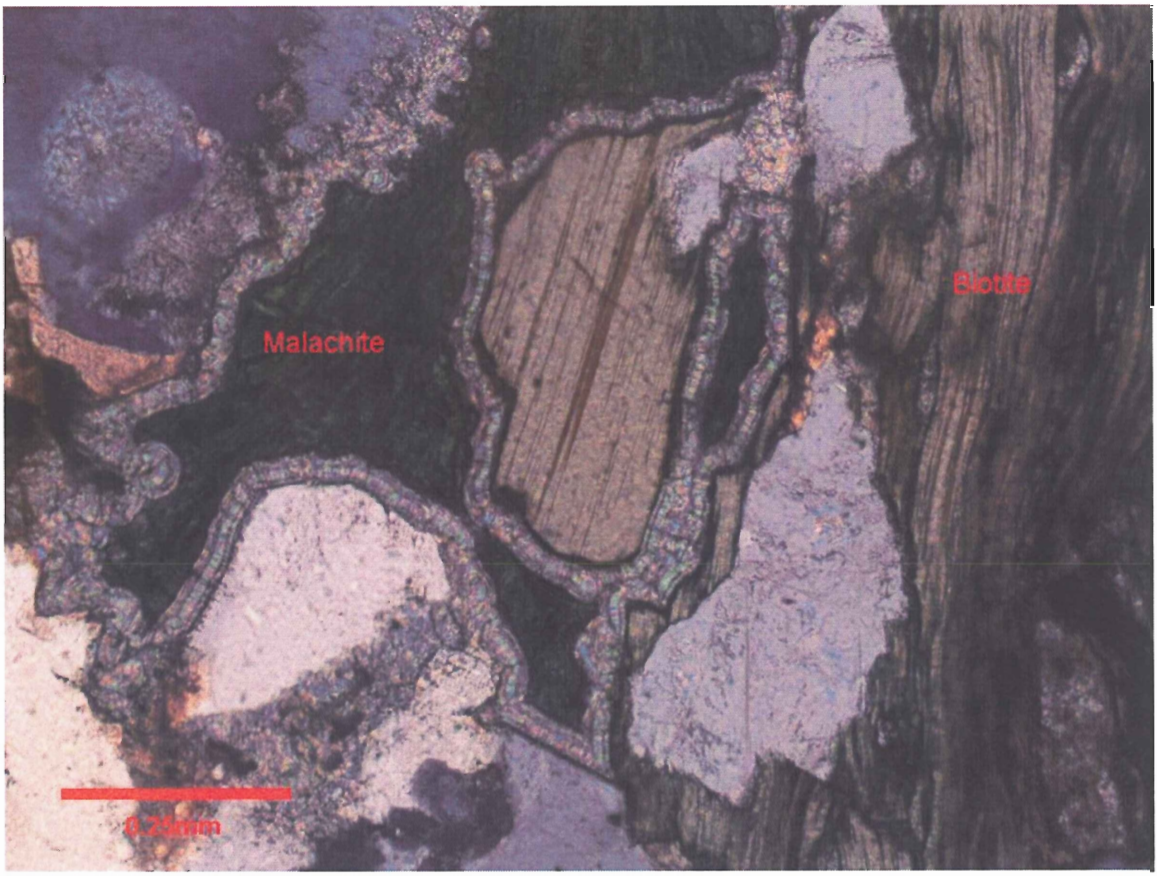

Figure 6.1: Sample AFI05, a carbonate (highly birefringent, probably calcite) rim is visible around malachite grains; some iron oxide-hydroxide is responsible for the reddish staining (e.g. near the scale bar in the figure). Sample AFI-05 is the only sample containing malachite rims. A strong foliation is defined by biotite.

From thin section analysis, the rocks containing copper mineralization can be described as porphyritic, foliated biotite granodiorite with a mineral assemblage of

plagioclase, quartz, potassium feldspar, biotite, magnetite, hematite, malachite and minor amounts of opaque minerals; one sample contains rimmed malachite. The rocks with no copper mineralization can be described as porphyritic hornblende ±biotite granodiorite with a mineral assemblage of plagioclase, quartz, potassium feldspar, hornblende, biotite, magnetite, hematite and minor amounts of opaque minerals.

Recrystallized quartz grains as well as undulose extinction in quartz grains are visible in all samples, indicating that these rocks have undergone strain. The rims of magnetite grains are partially oxidized to hematite during weathering.

6.2 Electron Microprobe

The electron microprobe analyses were done at Dalhousie University's Robert Mackay Laboratory. Microprobe analysis was used to confirm the identification of phases for petrography and to study variations in the mineral chemistry. A JEOL 733 electron microprobe with four wavelength dispersive spectrometers and an Oxford Link eXL energy dispersive system was used. The resolution of the energy dispersive detector was 137 V at 5.9 KV. Each spectrum was acquired for 40 seconds, with an acceleration voltage of 15 Kv and a beam current of 15 nA. Probe spot size was approximately 1 μm in diameter. Geological standards were used for controls. Analyses were carried out under the supervision of Dr. Patricia Stoffyn.

Electron microprobe analyses are given in Appendix 4. No sulphides were encountered in the thin or polished sections. Figure 6.2 shows an electron backscatter image of the common assemblage of minerals in the foliated, mineralized samples from the Ice property (sample 14b).

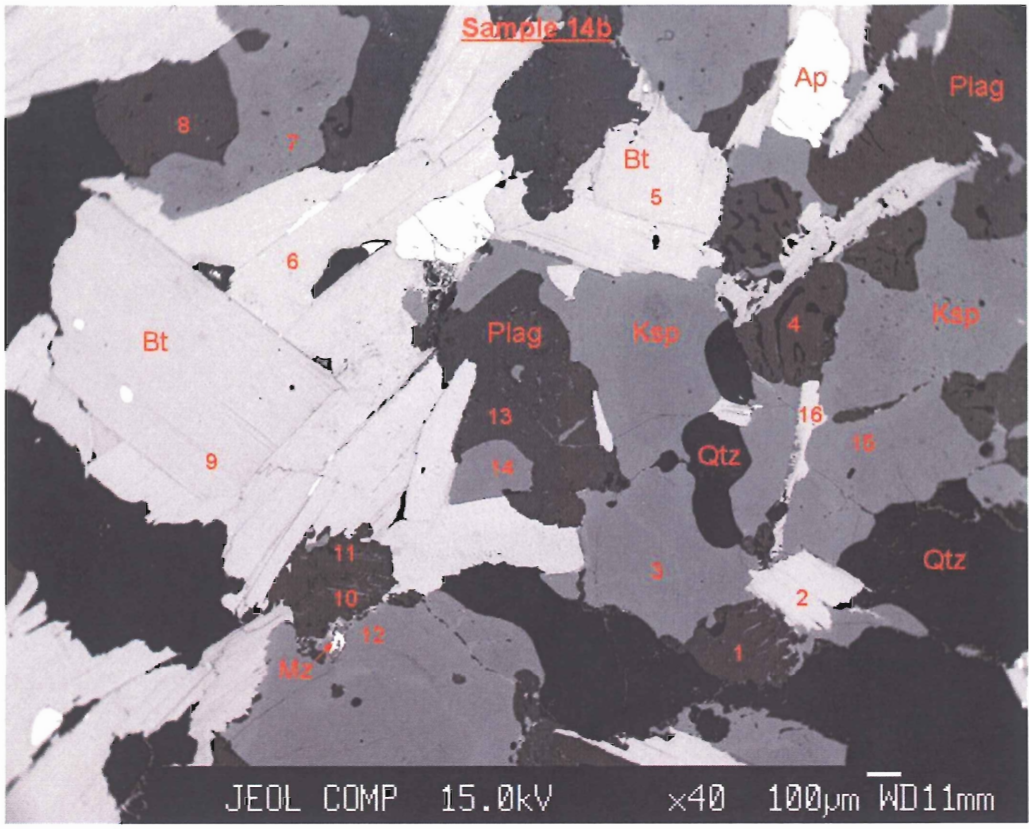

Figure 6.2: Backscatter electron image of sample 14b. Ap=Apatite, Bt=Biotite, Qtz=Quartz, Plag=Plagioclase, Ksp=Alkali feldspar, Mz=Monazite. Numbers refer to electron microprobe measurements located in appendix 4a (beginning with AFI-14b-1). 1=Plagioclase, 2=Biotite, 3=Alkali feldspar, 4=Plagioclase, 5=Biotite, 6=Biotite, 7=Alkali feldspar, 8=Plagioclase, 9=Biotite, 10=Plagioclase, 11=Quartz in Plagioclase, 12=Alkali feldspar, 13=Plagioclase, 14=Alkali feldspar, 15= Alkali feldspar, 16=Biotite.

Figure 6.3 shows an element map generated with the electron microprobe of S, Fe, Na, Si, and Cu to illustrate that there is no sulfur in the rocks of the Ice property. Copper minerals in the Ice samples come in at least two species, a Cu-Si-Fe bearing species (possibly chrysocolla) and a Cu species (probably malachite, as O and C are not analyzed for in the microprobe). From XRD analysis, the dominant copper mineral is confirmed to be malachite; chrysocolla is amorphous and generally yields no recognizable crystalline pattern in XRD.

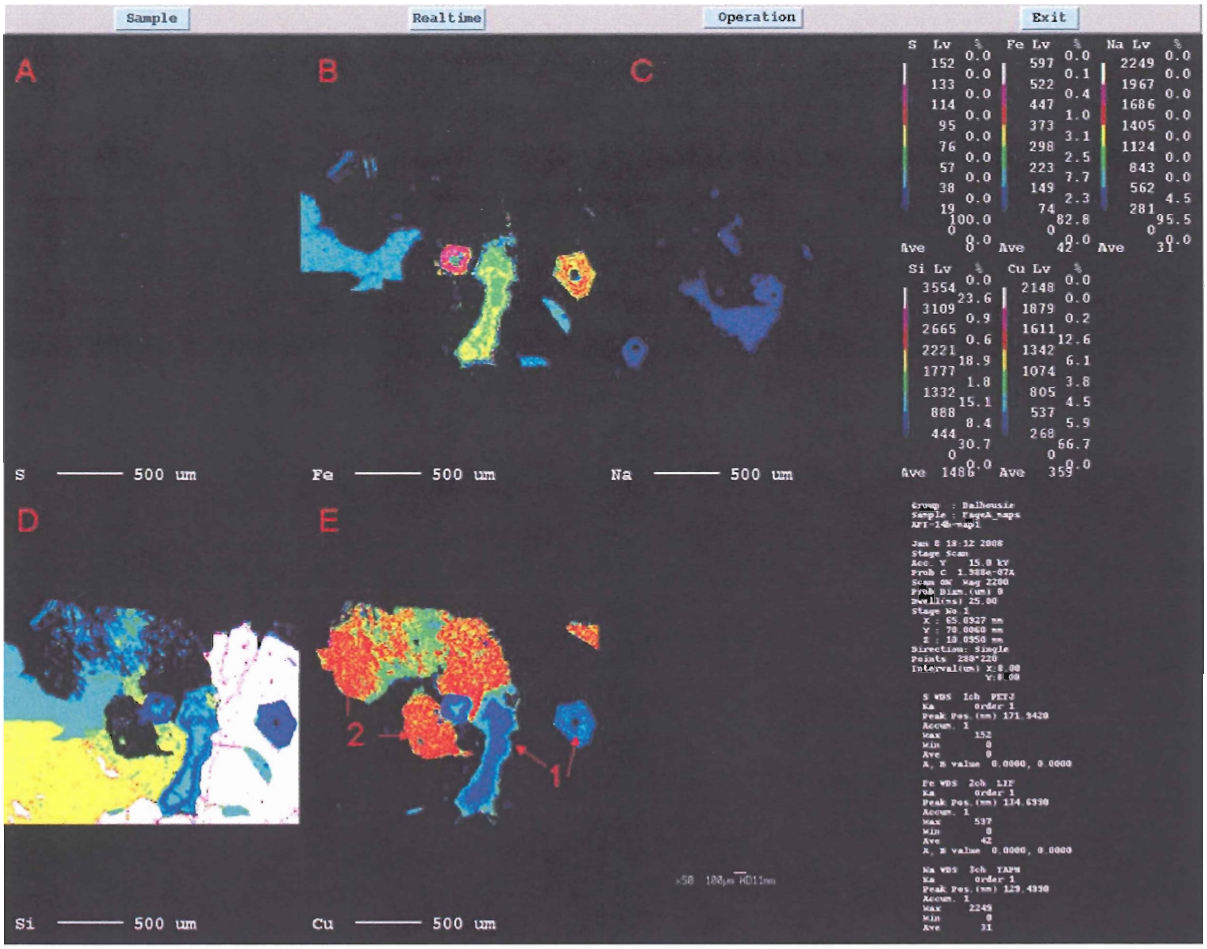

Figure 6.3: Element map from the electron microprobe. A-Sulfur, B-Iron, C-Sodium, D-Silicon, E-Copper. 1-Copper Silicate, 2-Copper Oxide. The copper minerals do not contain sulfur, and no sulphides were encountered in any microprobe analysis of Ice samples. The occurrence of remnant Fe associated with the Cu suggests that the copper oxides may be the oxidised equivalent of pre-existing sulphides (Sample AFI-14b)

Analyses of feldspars from the Ice samples, plotted on an Orthoclase-Albite-Anorthite diagram in figure 6.4, shows that the majority of k-feldspars are Or_{80-85}, and the majority of plagioclase are oligoclase, An_{30}. There are also a number of pure albite grains in the rocks.

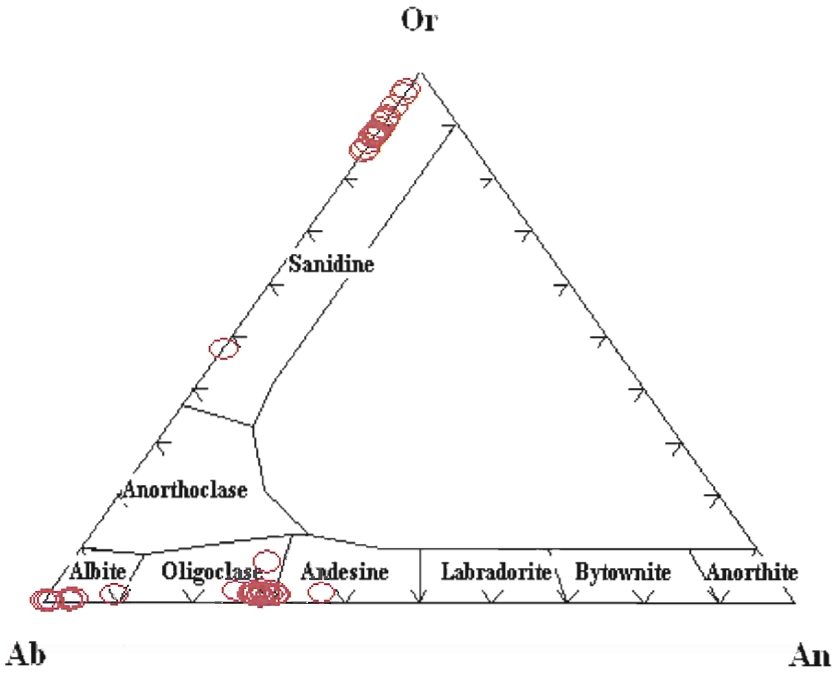

Figure 6.4: Analyses of feldspar grains from Ice samples plotted on an Orthoclase-Albite-Anorthite diagram.

A classification of the biotites analyzed with the electron microprobe is shown in figure 6.5.

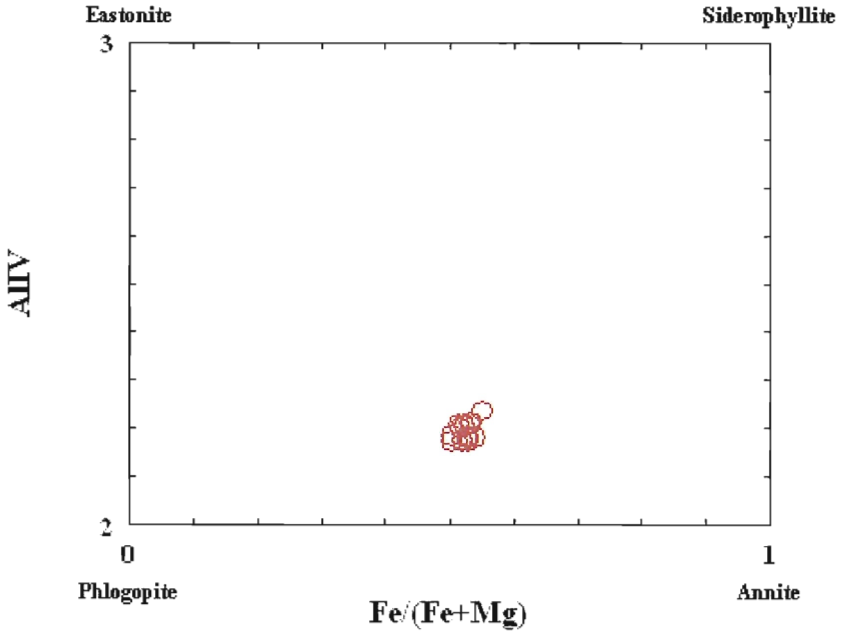

Figure 6.5: Classification of biotites as of intermediate composition from microprobe analyses.

6.3 X-ray Diffraction

Three samples from the Ice property were measured using X-ray diffraction to determine the identity of the green 'copper oxide' minerals. From the electron microprobe it is evident that there are at least two copper bearing phases, a Cu-Fe-Si bearing phase and a Cu-bearing phase (C and O are not analyzed for but are assumed to be present). From the X-ray diffraction analyses, the green mineral has been identified as malachite [$Cu_2(CO_3)(OH)_2$]. In samples AFI-05 and AFI-06 there was some contamination from other minerals (quartz and feldspars) in the diffractogram, but sample AFI-14 (Fig. 6.6) clearly shows the diffractogram for malachite.

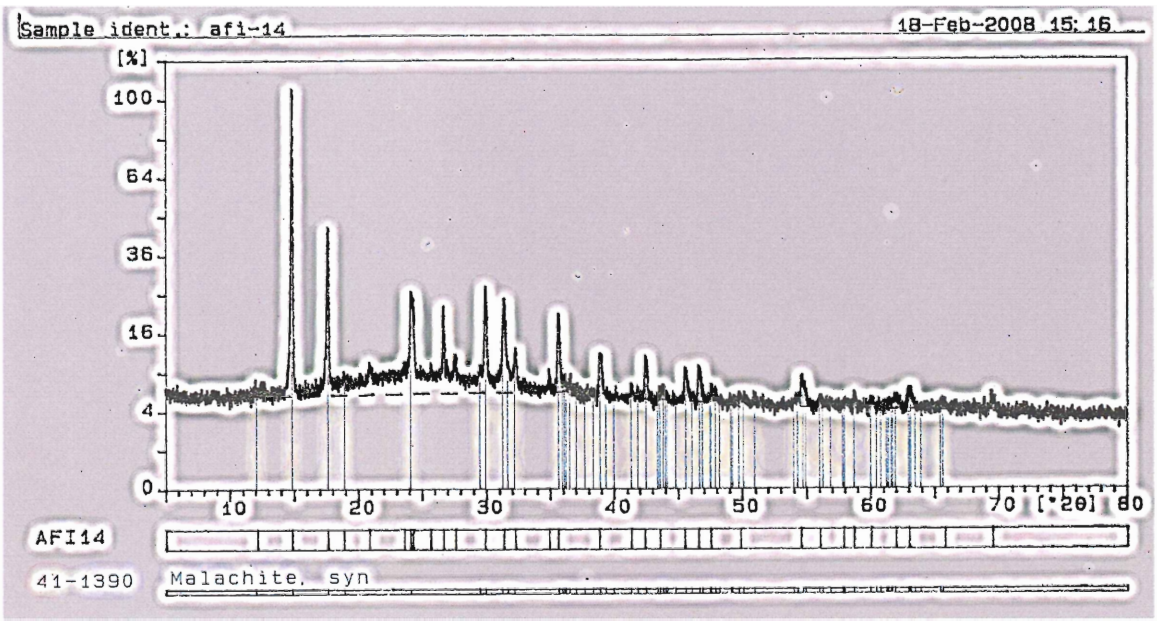

Figure 6.6: X-Ray Diffraction plot from sample AFI-14 showing the major peaks for malachite.

6.4 Interpretations

From thin section description, the Ice rocks are granodiorites, and from the textures observed, they have undergone strain and have been oxidized and weathered. Sulphides are not present in the Ice rock samples. Feldspars analysed in the Ice samples are sanidine with Or_{80-85}, Oligoclase and Albite. There are at least two copper minerals in

the Ice rocks, but malachite is the dominant copper mineral, whereas some indication of Chrysocolla (Cu silicate) was obtained though the microprobe.

Chapter 7

Genetic Model for the Ice Property

7.1 Model for Minto and Williams Creek

Previous workers have assigned the deposits of the Carmacks Copper Belt to various different deposit types, including metamorphosed volcanogenic massive sulphide deposits, metamorphosed redbed copper deposits and deformed copper-gold porphyries (Pearson and Clark, 1979). Tafti and Mortenson (2004) reported that the ore and alteration assemblages closely resemble those associated with early stages of mineralization in typical copper (-gold) porphyry deposits as well as some iron-oxide-copper-gold-type (IOCG) deposits. Supergene effects at Minto and Williams Creek are characterized by the presence of abundant secondary copper oxide minerals and less abundant secondary copper sulphide minerals and by the local presence of hematite and clays. Nearly all of the copper contained at the No. 1 zone at Williams Creek appears to occur in the form of secondary copper oxide minerals, and there is little evidence that significant amounts of hypogene sulphide minerals were ever present in the rocks (Tafti and Mortenson, 2004). They proposed a simple 'arrested porphyry' deposit model has been where the deposit formed as a porphyry system which stopped developing at some point. The extent of supergene enrichment at the Williams Creek suggests that it was the product of secondary oxide-mineral enrichment, and is not hypogene ore that has oxidized in place.

7.2 Exotic Deposits

Because the Ice mineralization has some characteristics of a transported or exotic copper deposit, the concept is introduced here. Exotic copper deposits are formed in association with the supergene oxidation and enrichment of porphyry copper deposits. Supergene alteration commonly involves vertical solution movement, but can also involve a horizontal component when copper-rich acidic solutions can migrate laterally. Depending on Eh and pH conditions, copper may be transported through paleodrainage networks over several kilometres from source and produce continuous copper mineralization. This copper mineralization is primarily deposited in oxide form but secondary sulphide copper may also be present close to the source (Munchmeyer, 1996).

Geomorphologic conditions and the chemical reactivity of host rocks and sediments influence the size and shape of exotic deposits. Exotic deposits mainly consist of oxidized copper minerals (silicates, chlorides, oxides, and carbonates) deposited into gravels and underlying bedrock of paleodrainages which carry the copper-bearing solutions. Copper may also precipitate as chalcocite on pyrite close to the source. In the Andean porphyry systems, exotic deposits were created in arid to semi-arid conditions (Munchmeyer, 1996). Figure 7.1 shows a schematic model of an exotic system.

For example, the Exotica deposit in Chile is located within a paleochannel that begins at the head of a paleodrainage located over the central portion of the Chuquicamata porphyry deposit and extends southward with a slope of 3 to 7 degrees over 6.5km. Its northern end is found within the Chuquicamata mine and its southern end is found beneath 200 m of gravels. The copper minerals are deposited within the base of the paleochannel and are composed of chrysocolla, copper wad (a copper-rich Mn-Fe oxide) and atacamite (Munchmeyer, 1996).

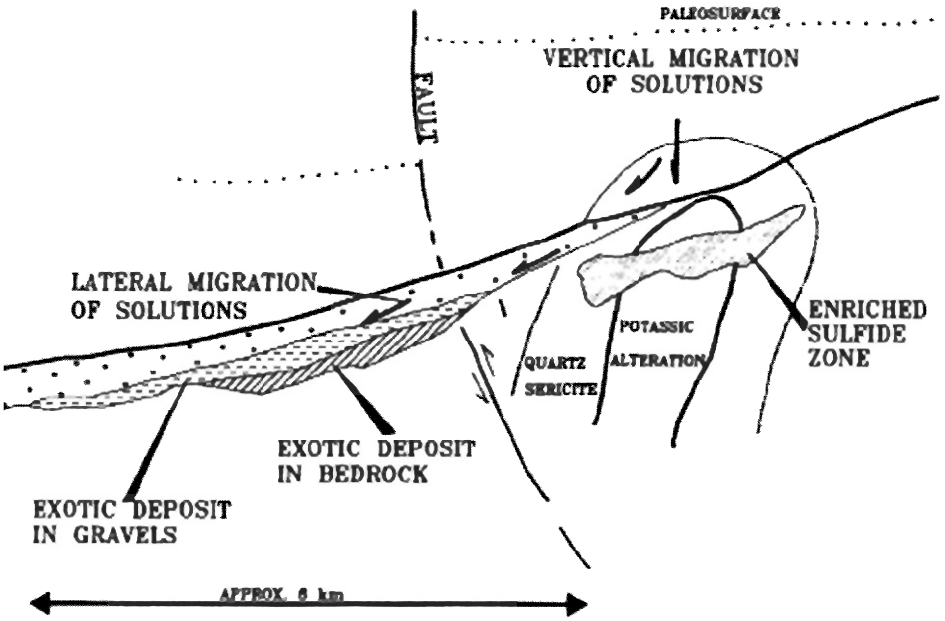

Figure 7.1: Representation of an exotic copper deposit and its relation to a porphyry copper deposit undergoing supergene enrichment (After Munchmeyer, 1996).

7.3 Porphyry Copper Deposits

Porphyry deposits are large, low to medium grade deposits where hypogene ore minerals are spatially and genetically related to felsic to intermediate porphyry intrusions and are often structurally controlled (Eckstrand et al. 1995). Porphyry copper deposits are associated with subduction of oceanic crust in both island arcs (Philippines) and at continental margins (North and South Cordillera). Supergene enrichment may occur by weathering of primary sulphides, creating zones of much higher copper grades, enhancing the possibility of economic exploitation (Eckstrand et al. 1995). Porphyry copper deposits range in size from tens of millions of tones of ore to billions of tones; with copper grades ranging from 0.2% to more than 1%.

The sequence of events that generates a porphyry deposit can be paraphrased as an intrusion followed by early marginal crystallization, producing a solid shell which

later ruptures to produce porphyritic-aphanitic textures in the crystallized rocks (Lowell and Guilbert, 1970). Volatiles are released due to quenching and migrate outward through stockwork and brecciated zones in the cool margins where alteration and mineralization occurs (Lowell and Guilbert, 1970).

Porphyry copper deposits are commonly rich in sulphur, with copper contained in chalcopyrite ($CuFeS_2$) and are associated with pyrite (FeS_2). Some porphyry copper deposits, however, contain much lower amounts of sulphur with the copper being contained primarily in bornite (Cu_5FeS_4) which has a lower S/(Fe+Cu) ratio.

A geologic report of the San Manuel-Kalamazoo deposit, Arizona, by Lowell and Guilbert (1970) illustrates the alteration and mineralization zoning found in porphyry deposits shown in figure 7.2. A potassic zone, near the centre of the deposit, is characterized by replacement of primary minerals by secondary biotite, K-feldspar, quartz, sericite, and to a lesser extent anhydrite. The potassic zone is characterized by a 1:2 pyrite:chalcopyrite ratio with about 0.5% copper; surrounding the potassic zone is an ore shell with a pyrite:chalcopyrite ratio of about 1:1 and 0.5-1% Cu. The phyllic zone is characterized by alteration minerals including quartz, sericite, pyrite, hydrous micas and minor chlorite and rutile. The argillic zone is characterized by pyrite and the alteration of plagioclase to clay minerals. Mineralization in the phyllic and argillic zones consists of a zone on the periphery of the ore shell with a 10:1 pyrite:chalcopyrite ratio with 0.1-0.5% Cu grading into a pyrite shell which contains 6-25% pyrite by weight. The propylitic zone is characterized by plagioclase either fresh or rimmed with clay minerals, biotite replaced by chlorite and carbonate, and minor epidote and calcite are also present (Lowell and Guilbert, 1970).

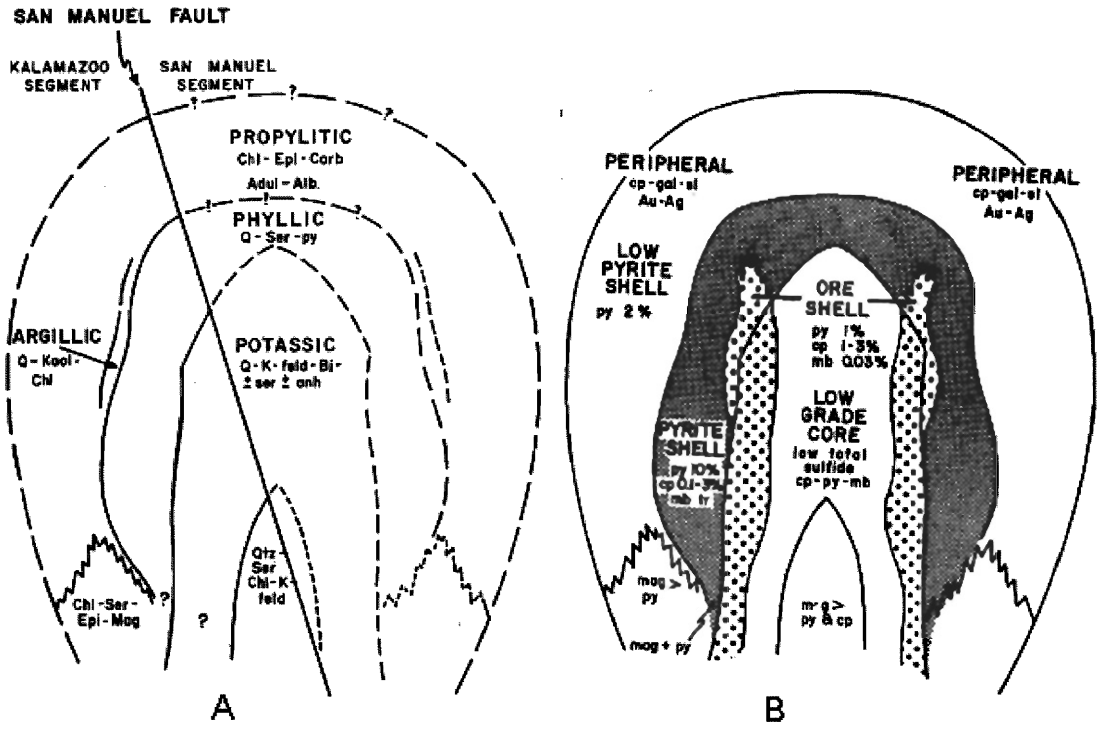

Figure 7.2: Concentric mineralization zones at the San Manuel-Kalamazoo Porphyry deposit. (A) Alteration zones. (B) Mineralization zones: py=pyrite, cp=chalcopyrite, mb=molybdenum, mag=magnetite, gal=galena (After Lowell and Guilbert, 1970).

7.4 Model for the Ice deposit

On the basis of observations at Ice, it seems that the deposit has properties of a porphyry type deposit, but the mineralization shows some characteristics of being transported from another place (exotic).

The Ice may be an exotic deposit because the rocks of the Ice contain no sulphur or obvious remnants of sulphides; all of the copper minerals are oxides or carbonates such as malachite and chrysocolla, which are both Cu minerals common in exotic deposits. The base of the deposit occurs as a coherent layer which may represent a paleo-water table. The deposit contains gold, up to 0.4 g/t, which cannot be mobilized into the

water table as easily as copper, and the potassic alteration in the ore zone is not part of the exotic deposit model.

Although the Ice contains no copper sulphides, the Cu carbonates and silicates in the mineralized vugs seem to contain remnants of Fe (Fig 6.3). The mineralized vugs may represent a dissolved hypogene mineral, which could well have been a sulphide of Fe and Cu. Ice also contains gold grades up to 0.4 g/t which are approaching the threshold between copper porphyry and copper-gold porphyry. The high copper grades and lack of sulphides at the Ice could represent in situ supergene enrichment at the top of an exposed porphyry copper deposit. The potassic alteration correlation with higher copper grades is a property of porphyry copper deposits, and is unlikely to be associated with an exotic deposit; an explanation why surface transported Cu would predominantly precipitate in the K_2O and Rb rich rocks is not forthcoming; not all exposed rocks containing biotite, or magnetite are mineralized.

The deposit model chosen by the writer for this deposit is a 'deformed porphyry' similar to the model proposed by Tafti and Mortenson (2004) for Minto and Williams Creek. The deposit was formed in a porphyry system which was later subjected to tectonic deformation, changing the shape of the orebody into a coherent layer as in the simplified process shown in figure 7.3.

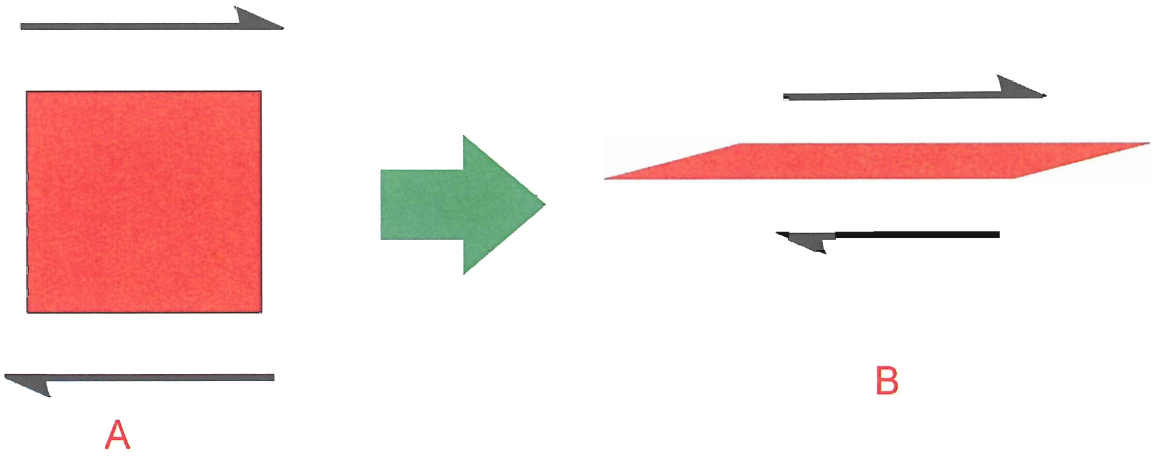

Figure 7.3: Simplified diagram (cross-section view) showing an orebody undergoing tectonic deformation.

It is proposed that the malachite and chrysocolla (?) found in the Ice rocks are found in situ; inhabiting the same space as sulphides before they were oxidized. The primary deposit is probably a low sulphur porphyry copper deposit with bornite being the major sulphide (much like Minto).

Chapter 8

Conclusions and Recommendations for Future Work

8.1 Discussion

If the Ice were formed as an exotic deposit, the Williams Creek deposit could be a candidate for the primary deposit because of its proximity to the ICE, but there are doubts whether it ever contained primary sulphide minerals as well (Tafti and Mortenson, 2004). The primary porphyry deposit could also be an undiscovered deposit buried below the surface or could have already been eroded away and destroyed. To explore for more exotic deposits in the area, it would be necessary to reconstruct the Tertiary paleotopography of a stream system and groundwater table connecting the Minto, Williams Creek and Ice.

It is concluded that the granodiorites of the Ice property have undergone tectonic strain and were crystallized at depths of >9km. Whatever the irregular shape of the original Cu-rich, K-feldspar and biotite porphyry, during deformation it has been transposed into a tabular body. To explore for more porphyry-type mineralization, it is suggested that airborne radiometric detection of potassium could be useful.

8.2 Suggestions for Future Work

1. Study of the vugs containing Cu minerals to deduce the pre-existing mineral dissolved to create the vug. It is suggested that microprobe maps of 50 or more vugs would give enough information to ascertain whether the dissolved minerals were Cu sulphides, pyrite or some other mineral phase.
2. Study of weathering surfaces and distribution of Cu as they may relate to a Tertiary paleosurface.

3. Sulphides should be found up or down foliation from the outcropping copper oxides. Mapping the structure of the area is recommended for future workers.
4. The results of the drilling and ICP/MMI soil geochemistry (valuable exploration tools) are not available to the author at this time, so these cannot be commented on in the context of exploration.
5. A radiometric survey to identify areas with elevated zones of potassium and rubidium.

8.3 Conclusions

The objectives of the thesis laid out in 1.5 have been met to some extent; comments follow.

1. To understand the correlation (or non-correlation) between magnetic anomalies and mineralization in the Ice area. Although there is abundant magnetite in various parts of the Ice deposit, no direct correlation exists with copper mineralization. It is possible that magnetite is more abundant in the biotite rich granodiorite, but magnetic anomalies do not necessarily correlate with higher copper grades.

2. To determine the relative timing of mineralization and regional deformation/metamorphism. This study concurs with previous authors that mineralization preceded deformation. The data are compatible with sulphide mineralization and potassic alteration having been formed at several kilometres depth and subsequently sheared, to be later exposed and oxidized by weathering near the surface.

3. A comparison of the mineralogy of alteration (feldspars and biotite). Due to the intense structural deformation, it was not possible to differentiate what is magmatic K-feldspar and magmatic biotite from (potassic) alteration equivalents in the rocks.

However, feldspar and biotite appear to be identical to those described at Minto and Williams Creek by other workers (Tafti and Mortenson, 2004).

4. To determine similarities/differences between the ICE and Minto/Williams Creek deposits. Ice has no sulphides, which is similar to Williams Creek, whereas Minto has remnants of Cu sulphides and pyrite. The deposits have a similar origin and Ice seems to have more analogies with Williams Creek.

5. To generate a genetic deposit model for the Ice deposit. The preferred model for Ice is formation of a porphyry type deposits with Cu and Au at several kilometres depth, accompanied by potassic alteration. Subsequently, shearing transformed the irregular deposit into tabular foliated bodies. Exposure to the surface during Tertiary exhumation may have eliminated many mineralized areas due to erosion, but also allowed the remnant copper and gold minerals to be weathered and oxidized. Lack of glaciation in the immediate area prevented the oxidized, possibly in part exotic copper minerals from being eroded.

Appendix 1
Rock Sample Descriptions

Samples with high copper concentrations are AFI-02 (11269ppm), AFI-5 (11126ppm), AFI-6 (14904ppm), and AFI-14 (10689ppm) which are above the upper limit level for XRF (10000ppm).

AFI-01
Granodiorite
Foliated
Porphyritic
Malachite ~ 1%
Plagioclase
Quartz (recrystallized?)
Potassium Feldspar
Biotite
Magnetite and Hematite

AFI-02
Granodiorite
Foliated
Porphyritic
0.5 cm pegmatitic vein cuts across sample
Malachite ~1%
Plagioclase
Quartz
Potassium Feldspar (Large phenocrysts 1-4cm)
Biotite
Magnetite and Hematite

AFI-03
Aplite Dyke
Aphanitic
3cm pegmatitic vein cuts across sample
Plagioclase >60%
Quartz
Potassium Feldspar
Biotite

AFI-04
Granodiorite
Massive
Porphyritic
Coarse grained (0.2-1cm)
Plagioclase
Quartz
Potassium Feldspar (Low Amounts)
Hornblende>>Biotite

AFI-05
Granodiorite
Foliated
Porphyritic
Malachite ~2%
Plagioclase
Potassium Feldspar
Plagioclase
Quartz
Biotite
Magnetite and Hematite

AFI-06
Granodiorite
Weakly foliated
Porphyritic
Pegmatitic
Malachite >2%
Potassium Feldspar
Plagioclase
Quartz
Magnetite and Hematite

AFI-07
Granodiorite
Massive
Porphyritic
Plagioclase
Quartz
Potassium Feldspar
Hornblende>Biotite
Magnetite and Hematite

AFI-08
Granodiorite
Possible weak foliation
Porphyritic
Plagioclase
Quartz
Potassium Feldspar
Biotite
Magnetite and Hematite

AFI-09
Granodiorite
Strongly Foliated
Porphyritic

Malachite >1%
Plagioclase
Potassium Feldspar
Quartz
Biotite
Magnetite and Hematite

AFI-10
Granodiorite
Foliated
Porphyritic
Plagioclase
Quartz
Potassium Feldspar
Biotite

AFI-11
Granodiorite
Porphyritic
Pegmatitic
Malachite<1%
Plagioclase
Quartz
Potassium Feldspar
Biotite
Magnetite and Hematite

AFI-12
Granodiorite
Strongly Foliated
Porphyritic
Malachite ~1%
Plagioclase
Quartz
Potassium Feldspar
Biotite
Magnetite and Hematite

AFI-13
Granodiorite
Strongly Foliated
Porphyritic
Malachite <1%
Plagioclase
Quartz
Potassium Feldspar
Biotite
Magnetite and Hematite

Appendix 3
XRF Geochemistry
Major elements

Sample ID	Al2O3	CaO	Fe2O3	K2O	LOI	MgO	MnO	Na2O	P2O5	SiO2	TiO2	Total
Units	wt%	wt%	wt%	wt%	wt%	wt%	wt%	wt%	wt%	wt%	wt%	wt%
Detect Limit	0.01	0.01	0.01	0.01	0.05	0.01	0.01	0.01	0.01	0.01	0.01	
AFI-2	15.04	2.27	4.17	3.88	1.41	1.47	0.06	3.18	0.24	65.65	0.37	97.75
AFI-3	18.92	3.66	2.37	1.26	0.47	0.8	0.04	5.83	0.09	66.58	0.31	100.3
AFI-4	16.69	3.79	4.23	1.54	0.57	1.43	0.07	4.64	0.21	67.01	0.42	100.6
AFI-5	16.54	1.89	5.44	5.67	1.93	1.78	0.09	3.26	0.28	61.15	0.52	98.55
AFI-6	18.6	3.1	5.35	5.56	4.81	1.94	0.09	2.94	0.26	54.22	0.55	97.42
AFI-7	17.77	4.56	3.95	2.02	2.34	1.32	0.09	5	0.19	63.57	0.38	101.2
AFI-8	16.74	3.66	4.89	1.85	1.19	1.71	0.08	4.48	0.32	65.3	0.48	100.7
AFI-10	16.2	3.21	4.05	2.63	0.53	1.72	0.06	4.02	0.27	67.59	0.45	100.7
AFI-12	16.09	2.48	4.88	3.95	1.46	1.7	0.07	3.32	0.24	65.43	0.43	100.1
AFI-14	12.58	1.27	4.19	5.56	1.03	1.32	0.06	1.86	0.21	70.13	0.34	98.55

Trace Elements

Sample ID	Ag	As	Ba	Bi	Co	Cr	Cu	Mo	Nb	Ni	Pb	Rb
units	ppm	ppm	ppm	ppm	ppm	ppm	ppm	ppm	ppm	ppm	ppm	ppm
AFI-2	0	2	2234	0	11	26	11269	12	8	0	6	96
AFI-3	0	0	560	0	0	12	45	1	2	2	0	44
AFI-4	0	0	548	0	11	18	153	1	9	4	3	71
AFI-5	0	5	4822	0	29	20	11126	2	9	3	11	124
AFI-6	7	13	3148	0	22	10	14904	3	12	0	10	122
AFI-7	0	0	1657	0	8	17	20	1	8	3	4	36
AFI-8	0	1	638	0	11	17	222	0	8	4	3	74
AFI-10	0	0	1638	0	7	17	956	1	7	3	4	85
AFI-12	0	3	2169	0	15	17	3739	5	9	3	6	110
AFI-14	5	2	4650	0	11	20	10689	2	6	0	8	123

Sample ID	Sn	Sr	Th	U	V	Y	Zn	Zr
units	ppm	ppm	ppm	ppm	ppm	ppm	ppm	ppm
AFI-2	5	665	8	0	76	8	102	97
AFI-3	0	1226	7	0	34	1	44	131
AFI-4	0	766	8	0	76	5	64	138
AFI-5	5	756	7	0	112	7	99	144
AFI-6	5	723	7	0	99	9	101	148
AFI-7	0	946	4	0	66	12	55	121
AFI-8	0	783	9	0	92	6	84	131
AFI-10	0	783	7	0	85	7	74	126
AFI-12	0	655	8	0	85	8	102	110
AFI-14	7	592	5	0	74	9	69	90

Appendix 4a: Silicate Microprobe data (Mass Percent).

ID	Mineral	K2O	Cr2O3	Na2O	Al2O3	MnO	CaO	TiO2	MgO	SiO2	FeO	Total
AFI03b-01	Magnetite (core)	0.0643	0.2747	0	0.1356	0.3053	0.0784	0.2498	0.0182	0.0922	91.9954	93.214
AFI03b-2	Magnetite (rim)	0.0834	0.2447	0.002	0.113	0.1893	0.0609	0.2596	0	0.1072	88.5438	89.604
AFI03b-3	Plagioclase	0.3667	0	8.0637	24.5034	0	5.5181	0	0	60.9405	0.0565	99.449
AFI03b-4	K Feldspar	15.3117	0	0.4554	18.9799	0	0.0293	0.0295	0	62.9226	0.0345	97.763
AFI03b-5	Plagioclase(core)	0.3802	0	8.3108	24.4593	0	5.098	0	0	61.8417	0.074	100.1639
AFI03b-6	Plagioclase (rim)	0.2401	0	8.4001	24.5278	0	5.1297	0	0	62.1241	0.044	100.4657
AFI03b-7	K Feldspar	14.4075	0.0055	0.882	18.344	0	0	0.0913	0	58.4504	0.0474	92.2282
AFI03b-8	Biotite	9.1751	0.0546	0.1014	15.3892	0.3967	0.0414	3.0592	9.898	35.2244	19.6907	93.0308
AFI03b-9	Titano-magnetite	0.1376	0.2095	0.0595	2.4159	0.1196	0.3209	5.9015	0.8594	4.365	74.9205	89.3095
AFI03b-10	Biotite	8.6243	0.0538	0.0912	15.6303	0.3925	0.1252	2.5464	10.8515	35.7319	19.2861	93.3333
AFI03b-12	Plagioclase	0.2451	0	8.1044	23.8201	0	5.4913	0	0	58.8764	0.0515	96.5889
AFI04-01	K Feldspar	14.3548	0.0177	1.1009	18.8057	0	0.0432	0.0269	0	61.9443	0.0349	96.3285
AFI04-2	Plagioclase	0.1309	0	10.0544	20.4136	0	0.5537	0	0	67.897	0	99.0497
AFI04-3	Biotite	0.1987	0.0399	0.0062	17.4266	0.6096	0.2421	0.44	14.181	27.5949	24.4938	85.2328
AFI04-6	Biotite	0.0308	0.0484	0.0116	17.6431	0.652	0.0422	0.0537	14.683	27.0921	25.5961	85.8531
AFI04-7	Rutile	0.2534	0.1156	0.0526	1.7646	0.0525	0.6745	75.6768	0.138	8.5395	2.6911	89.9587
AFI04-8	K Feldspar	13.8094	0	1.4054	18.578	0	0.0153	0.0431	0	60.9429	0.0195	94.8137
AFI04-9	Plagioclase	0.1201	0	10.0239	20.2372	0	0.6802	0	0	67.3491	0	98.4106
AFI04-10	Plagioclase	0.0473	0	10.312	19.7348	0	0.0177	0	0	67.5835	0	97.6954
AFI04-12	Biotite	0.0686	0.0291	0.0075	16.8687	0.606	0.7927	1.2882	13.1432	26.0244	23.5256	82.3541
AFI04-13	Biotite	3.2039	0.0514	0.0463	15.2815	0.4311	0.1723	2.244	12.0104	28.6855	21.3187	83.4452
AFI04-14	Biotite	0.0483	0.031	0.0158	17.8004	0.6204	0.1918	0.3474	13.627	26.4251	24.7575	83.8648
AFI11-03	Biotite	8.8087	0	0.092	15.9479	0.4637	0.0239	2.877	10.7306	36.4496	20.5126	95.9061
AFI11-4	K Feldspar	0.0155	0	0.0148	0.0188	0	0	0	0.0129	97.2498	0	97.3119
AFI11-5	K Feldspar	14.3273	0	1.2186	19.2693	0	0.0082	0	0	63.7539	0.0225	98.5999
AFI11-6	K Feldspar	14.0619	0	1.2737	19.3067	0	0.0226	0.0006	0.0067	63.1632	0.0235	97.8589
AFI11-7	K Feldspar	14.09	0	1.2212	19.3161	0	0.0049	0.0413	0	63.3824	0.0304	98.0864
AFI11-8	Biotite	8.787	0	0.0803	15.4593	0.4906	0.0376	2.926	10.3644	36.1973	20.3776	94.7202
AFI11-9	Plagioclase	0.224	0	7.4703	24.5229	0	5.2244	0	0.0104	60.1377	0.019	97.6087
AFI11-10	Plagioclase	1.6951	0	8.6549	21.1979	0	1.5409	0	0	66.2942	0	99.383

ID	Mineral	K2O	Cr2O3	Na2O	Al2O3	MnO	CaO	TiO2	MgO	SiO2	FeO	Total
AFI11-11	Plagioclase	0.336	0	7.6689	25.3742	0	5.9169	0	0	60.7824	0.053	100.1313
AFI11-12	Plagioclase	0.3168	0	7.8729	25.5915	0	5.8487	0	0	61.1577	0.0465	100.834
AFI11-13	K Feldspar	14.5586	0	0.9677	19.3852	0	0.0017	0.0569	0.0041	63.5635	0.0354	98.5732
AFI16-2	Chlorite	8.8519	0.0256	0.1333	15.9711	0.3854	0.0803	2.3536	9.4307	36.1107	21.4817	94.8243
AFI16-3	K Feldspar	14.4853	0	0.825	19.3005	0	0.0152	0.05	0	62.4088	0.0225	97.1074
AFI16-4	K Feldspar	14.1916	0	0.9028	19.4515	0	0.0165	0.1364	0.0069	62.0636	0.005	96.7743
AFI-04A-1	Plagioclase	0.2058	0	7.8325	23.6689	0	6.0029	0	0	57.5954	0.0806	95.3861
AFI-04A-2	K Feldspar	14.3211	0	0.3483	18.145	0	0.0042	0.0737	0	60.585	0	93.4773
AFI-04A-4	Biotite	9.1836	0.0423	0.107	15.7487	0.4656	0.0235	2.8893	10.9461	36.5025	19.6084	95.5171
AFI-04A-5	Plagioclase	0.1764	0	8.093	24.8834	0	5.9025	0	0	60.8707	0.1997	100.1256
AFI-04A-6	K Feldspar	14.4816	0	0.8879	19.0502	0	0	0.0347	0	63.397	0.1265	97.978
AFI-04A-7	Biotite	8.8647	0.0123	0.0899	15.8106	0.46	0.0952	3.1528	10.4593	36.2205	19.8156	94.9809
AFI-04A-8	Biotite	9.0395	0	0.0656	15.6353	0.4886	0.0186	2.9325	10.5596	36.3708	20.1121	95.2227
AFI-04A-9	Plagioclase	0.1461	0	8.1461	25.071	0	5.8128	0	0	61.3819	0.0737	100.6315
AFI-04A-10	K Feldspar	14.3052	0.0035	0.9451	19.0353	0	0	0.0254	0	63.6248	0.0227	97.9621
AFI-04A-11	Plagioclase (rim)	0.2423	0	7.8922	25.4191	0	6.241	0	0	60.7882	0.13	100.7127
AFI-04A-12	Plagioclase(core)	3.8846	0	5.4069	22.6867	0	4.0336	0	1.5741	51.6056	2.9157	92.1073
AFI-04A-13	Biotite	9.1977	0.0314	0.0813	15.3789	0.4673	0.0041	2.8515	10.2542	35.9885	19.9941	94.2491
AFI-04A-14	Biotite	9.0966	0.0529	0.127	15.5252	0.5343	0.0644	2.8485	10.2857	36.5432	20.6223	95.7002
AFI-04A-15	Plagioclase	0.2842	0	7.13	26.4069	0	7.5176	0	0	58.7881	0.0574	100.1842
AFI-04A-16	Plagioclase	0.3992	0	7.9953	25.0089	0	5.8294	0	0	61.2737	0.087	100.5934
AFI-04A-17	K Feldspar	14.8135	0	0.6979	19.1631	0	0.0065	0.0669	0	63.2337	0.0543	98.0359
AFI-04A-18	K Feldspar	14.4642	0	0.9228	19.1792	0	0	0.0656	0	63.5129	0.0375	98.1823
AFI-05b-1	Plagioclase	0.0439	0	10.9671	19.9042	0	0.1585	0	0	68.0952	0.0054	99.1744
AFI-05b-2	K Feldspar	13.8037	0	1.2893	19.1882	0	0.0368	0.0631	0	63.0699	0.0375	97.4886
AFI-05b-3	K Feldspar	13.7309	0	1.4131	19.0274	0	0.0194	0.0916	0	63.1927	0.0193	97.4945
AFI-05b-4	Biotite	9.1138	0.0392	0.1383	15.951	0.5229	0.0063	3.1202	10.5482	36.3374	19.6682	95.4455
AFI-05b-5	K Feldspar	13.2363	0	1.5387	19.0805	0	0.0221	0.068	0	63.5155	0.038	97.4992
AFI-05b-6	K Feldspar	13.8192	0	1.3639	19.1736	0	0.0171	0.0514	0	63.1901	0.0445	97.6599
AFI-05b-7	Biotite	9.3311	0.0468	0.098	15.7647	0.4662	0.0133	3.0899	9.9207	36.1171	21.4993	96.3472
AFI-05b-8	K Feldspar	13.9843	0	1.218	19.0028	0	0	0.0607	0	63.366	0.0459	97.6778
AFI-05b-9	K Feldspar	13.9898	0	1.1719	19.1663	0	0.0153	0.0489	0	63.5951	0.0331	98.0205

ID	Mineral	K2O	Cr2O3	Na2O	Al2O3	MnO	CaO	TiO2	MgO	SiO2	FeO	Total
AFI-05b-10	Biotite	2.3145	0.0078	0.0406	16.6659	0.5752	0.0826	0.9841	13.9882	30.5006	22.0338	87.1934
AFI-05b-11	K Feldspar	13.5029	0	1.4987	19.1754	0	0.0331	0.0557	0	63.1898	0.0494	97.5051
AFI-05b-12	K Feldspar	14.0476	0	1.2185	19.2476	0	0.0409	0.0551	0	63.6381	0.0158	98.2637
AFI-05b-13	Plagioclase	0.0443	0	11.1342	19.6793	0	0.108	0	0	68.8501	0	99.8159
AFI-05b-14	Plagioclase	0.0168	0	11.1774	19.922	0	0.0229	0	0	68.8159	0	99.9551
AFI-05b-15	Biotite	9.1437	0.0123	0.0949	15.4333	0.4893	0.0089	3.1337	10.5606	35.9673	19.5258	94.3699
AFI-05b-16	K Feldspar	13.8621	0	1.2726	19.0357	0	0.0295	0.0309	0	63.3935	0.0415	97.6658
AFI-05b-17	Plagioclase	0.03	0	10.8896	19.7588	0	0.1773	0	0	67.6876	0	98.5434
AFI-05b-18	K Feldspar	13.8529	0	1.2797	18.9899	0	0.0171	0.0563	0	63.0118	0.2241	97.4319
AFI-05b-19	Biotite	2.9971	0.0138	0.0528	16.6301	0.5944	0.0722	1.8853	13.792	31.4396	21.8574	89.3348
AFI-14b-1	Plagioclase	0.2658	0.0276	8.0065	24.5719	0	5.7173	0	0.0009	62.4087	0.0932	101.0919
AFI-14b-2	Biotite	9.4101	0.0956	0.0779	15.7992	0.4657	0.0362	2.5666	10.3965	36.4556	20.9865	96.29
AFI-14b-3	K Feldspar	13.9093	0.0572	1.2446	19.067	0.0117	0.0096	0.0881	0.0033	62.9119	0.0728	97.3756
AFI-14b-4	Plagioclase	0.2245	0.0012	8.065	24.7155	0	5.8024	0	0	60.8401	0.1656	99.8144
AFI-14b-5	Biotite	9.1869	0.0978	0.0794	15.9179	0.471	0.0233	2.7455	10.0376	36.3644	20.6373	95.5611
AFI-14b-6	Biotite	9.3585	0.0911	0.0934	16.067	0.4795	0.0057	2.9323	10.453	36.4919	20.186	96.1585
AFI-14b-7	K Feldspar	13.969	0.0397	1.2468	18.9471	0.0165	0	0.0887	0.0063	63.1836	0.0644	97.5621
AFI-14b-8	Plagioclase	0.2365	0.0174	7.8182	25.3025	0	6.3131	0	0	60.5181	0.0902	100.2959
AFI-14b-9	Biotite	9.11	0.0693	0.1168	15.5873	0.4462	0.0242	2.8458	10.4744	35.9889	20.2608	94.9238
AFI-14b-10	Plagioclase	0.2739	0.0109	8.159	24.4421	0	5.6158	0	0	61.124	0.1026	99.7284
AFI-14b-11	Quartz	0.0296	0	0.0091	0.0166	0	0.0067	0	0.0009	97.5949	0.0525	97.7104
AFI-14b-12	K Feldspar	13.9218	0.0188	1.205	19.1089	0.0149	0.0294	0.0906	0.0111	62.9645	0.0738	97.4389
AFI-14b-13	Plagioclase	0.2456	0	8.0113	24.7363	0	5.9983	0	0	60.9092	0.0917	99.9924
AFI-14b-14	K Feldspar	14.0415	0.0549	1.1695	18.8479	0.0186	0.016	0.0949	0.0039	63.156	0.0832	97.4865
AFI-14b-15	K Feldspar	13.9327	0.0216	1.2889	18.8609	0.0106	0.0096	0.059	0.0089	63.6263	0.0713	97.8899
AFI-14b-16	Biotite	9.5128	0.094	0.1042	15.9766	0.4618	0.0145	2.4696	10.4749	36.5964	20.549	96.2539
AFI-14b-17	K Feldspar	14.0674	0.0244	1.1947	18.8968	0.0117	0.0404	0.0999	0.0087	63.0061	0.0763	97.4265
AFI-14b-18	Plagioclase	0.0188	0	0.0231	0	0	0	0	0.0133	97.4568	0.0005	97.5126
AFI-17b-1	K Feldspar	14.6454	0.0605	0.6809	18.9432	0.0096	0.0091	0.0795	0	63.1086	0.059	97.5959
AFI-17b-2	Plagioclase	0.2858	0	8.6989	23.7777	0.0005	4.6886	0	0	62.4789	0.0912	100.0216
AFI-17b-3	Biotite	9.0899	0.1228	0.0746	16.3714	0.5549	0.0643	2.7645	9.3806	36.3132	20.9476	95.6839
AFI-17b-4	Biotite	8.8542	0.0936	0.0782	16.7348	0.4608	0.0414	2.2487	9.4698	36.543	21.3998	95.9244

ID	Mineral	K2O	Cr2O3	Na2O	Al2O3	MnO	CaO	TiO2	MgO	SiO2	FeO	Total
AFI-17b-5	Biotite	9.3138	0.079	0.0851	16.2775	0.4785	0.0242	2.3293	9.9012	35.4323	20.9665	94.8875
AFI-17b-6	Plagioclase	0.2214	0.0031	8.3785	24.3068	0	5.2133	0	0	61.4392	0.053	99.6154
AFI-17b-7	Plagioclase	0.3002	0	8.8662	23.1793	0.0069	4.5034	0	0	62.9023	0.0822	99.8406
AFI-17b-8	K Feldspar	14.2017	0.0077	1.1121	18.8778	0.0101	0.0234	0.0663	0.0013	63.3557	0.0218	97.6779
AFI-17b-9	K Feldspar	14.5376	0.0216	1.0796	18.6358	0.0053	0	0.0347	0.0063	64.2458	0.049	98.6158
AFI-17b-12	Biotite	3.4739	0.0949	0.053	17.1752	0.3885	0.1005	1.8092	10.8021	31.7968	26.2075	91.9016
AFI-17b-13	Plagioclase	0.6164	0.0095	7.6859	25.1774	0	3.8321	0	0.0185	61.4386	0.105	98.8835
AFI-17b-14	K Feldspar	14.3712	0.0345	0.8649	19.0084	0.0069	0.0123	0.0862	0.0028	63.142	0.0688	97.5981
AFI-18-1	Biotite	8.9743	0.0977	0.1103	15.9998	0.5608	0.1507	2.8032	9.6052	35.5843	20.1813	94.0677
AFI-18-2	Biotite	9.2573	0.0998	0.1051	16.0821	0.5504	0.0136	2.8751	9.6118	36.2058	20.7296	95.5306
AFI-18-3	Plagioclase	0.238	0.0017	8.5209	24.0692	0	4.997	0	0	61.8723	0.2144	99.9136
AFI-18-4	Plagioclase	0.2914	0	8.5099	23.9247	0	4.8542	0	0	62.189	0.0946	99.8638
AFI-18-5	K Feldspar	0.4076	0.0044	8.5996	23.6887	0.0053	4.5675	0	0	62.3391	0.1228	99.7351
AFI-18-6	Plagioclase	0.0279	0	0	0	0	0	0	0.0248	96.3286	0.011	96.3923
AFI-18-7	K Feldspar	0.1747	0.0155	8.437	24.0559	0	4.651	0	0	62.2876	0.1203	99.7421
AFI-18-8	K Feldspar	0.1608	0.004	8.6229	24.036	0	4.87	0	0	61.6369	0.1416	99.4723
AFI-18-9	Plagioclase	0.3118	0.0123	8.2729	24.3165	0	4.9109	0.0043	0	62.9636	0.1748	100.967
AFI-18-10	Biotite	9.078	0.1042	0.1122	16.1236	0.5871	0.0526	3.1603	9.4716	36.1051	20.5702	95.3649
AFI-18-11	Biotite	9.1112	0.0957	0.125	16.0948	0.5894	0.0302	2.8817	9.7212	35.9979	20.0832	94.7303
AFI-18-12	Biotite	8.7219	0.0839	0.1674	16.0128	0.5796	0.042	2.9206	9.7162	35.7742	20.042	94.0607
AFI-18-13	Biotite	9.0581	0.1042	0.1489	16.1415	0.5865	0.0314	3.0316	9.6481	36.2102	20.7888	95.7494
AFI-18-14	Plagioclase	0.3364	0.0119	8.5851	23.8984	0.009	4.5467	0	0	62.4362	0.1079	99.9317

ID	Mineral	K2O	Cr2O3	Na2O	Al2O3	MnO	CaO	TiO2	MgO	SiO2	FeO	CuO	Total
AFI-05b-20	Cu Silicate	0.0922	0	0.0646	3.1349	0.0061	1.0068	0.056	0.1992	30.0635	0.4632	43.6159	78.7024
AFI-05b-21	Cu Silicate	0.0891	0.0084	0.0969	4.838	0	1.1266	0.0902	0.327	42.0093	0.5396	44.2088	93.334

Appendix 4b: Microprobe data for geobarometry and Geothermometry (Mass Percent)

ID	Mineral	SiO2	TiO2	Al2O3	Cr2O3	FeO	MnO	MgO	CaO	Na2O	K2O	Total
AFI07-1	Hornblende	38.9853	0.7378	11.0786	0	16.7526	0.775	8.4188	9.2744	1.4767	1.0816	88.5809
AFI07-2	Hornblende	41.5823	0.7916	11.1768	0.0526	19.5543	0.6295	8.869	11.649	1.5176	1.372	97.1947
AFI07-3	Plagioclase	62.2732	0	23.0281	0	0.3439	0	0	5.0781	7.3154	1.4687	99.5075
AFI07-4	Plagioclase	61.4329	0	23.725	0	0.1618	0	0	5.7203	8.3957	0.2284	99.6642
AFI07-5	Plagioclase	64.1809	0	23.0166	0	0.0309	0	0	3.3453	7.6086	0.5688	98.7512
AFI07-6	Plagioclase	62.3548	0	24.1027	0	0.1309	0	0	5.7121	8.2686	0.3145	100.8835
AFI07-7	Hornblende	41.4231	0.8167	11.1545	0.0516	19.437	0.6933	8.8425	11.7558	1.402	1.39	96.9665
AFI07-8	Hornblende	40.9219	0.8116	11.6761	0.0459	19.794	0.6791	8.805	11.6476	1.5178	1.5146	97.4137
AFI07-9	Plagioclase	61.9124	0	23.5481	0	0.166	0.0028	0	5.4578	8.5452	0.1446	99.777
AFI07-11	Plagioclase	61.9682	0	23.7164	0	0.041	0	0	5.6189	8.4001	0.1595	99.9042
AFI07-12	Hornblende	41.6392	0.7953	11.3346	0.0196	19.4018	0.6869	9.032	11.5952	1.5399	1.4381	97.4827
AFI07-13	Hornblende	40.6924	0.9383	14.3734	0.0253	17.8439	1.3139	7.2719	8.7908	1.209	1.312	93.771
AFI07-14	Hornblende	41.5018	0.8004	11.4925	0.0305	19.4899	0.6701	8.7606	11.8835	1.4189	1.337	97.3853
AFI07-15	Plagioclase	61.9068	0	23.7386	0	0.1272	0	0	5.3558	8.5733	0.2724	99.9742
AFI07-16	Hornblende	41.7363	1.2677	11.9831	0.0527	18.9018	0.6455	8.9359	11.8417	1.4869	1.4064	98.2581
AFI07-17	Plagioclase	62.0568	0	24.0041	0	0.1491	0	0	5.2422	8.4208	0.1959	100.0688
AFI07-18	Hornblende	40.5883	0.9038	11.7061	0.0422	20.1063	0.6977	8.7765	11.6742	1.5721	1.6094	97.6767
AFI07-19	Hornblende	40.4636	0.8678	11.8166	0.0426	19.7744	0.7061	8.5297	11.5026	1.6692	1.626	96.9986
AFI07-20	Hornblende	37.5557	0.8927	10.8207	0.0538	20.0687	0.703	8.5048	11.5113	1.4953	1.5454	93.1515
AFI07-21	Hornblende	40.7297	0.8279	11.3804	0.0408	19.8758	0.6431	8.73	11.7619	1.4153	1.3567	96.7617
AFI07-24	Plagioclase	59.6623	0	23.3384	0	0.3609	0	0.02	5.2906	7.6239	0.5096	96.8058
AFI07-25	Hornblende	41.0899	0.8885	10.9058	0.0352	19.3436	0.6191	9.2919	11.7708	1.4151	1.2924	96.6524
AFI07-26	Hornblende	41.8919	0.7714	11.9489	0.0578	19.5104	0.656	8.4573	11.8948	1.2939	1.4647	97.9472
AFI07-27	Hornblende	40.7096	0.4205	13.2581	0.0041	19.249	0.521	9.2996	8.1672	0.9187	1.169	93.7169
AFI07-28	Plagioclase	61.5185	0	23.8841	0	0.0772	0	0	5.6489	8.3567	0.2182	99.7037
AFI07-29	Plagioclase	61.8415	0	23.7203	0	0.1673	0	0	5.5382	8.4776	0.1688	99.9137
AFI07-30	Hornblende	42.2584	0.8203	11.1522	0.0202	18.9533	0.6168	9.3726	11.7355	1.4952	1.3353	97.7599
AFI07-31	Hornblende	41.1114	0.9107	11.5402	0.0239	19.5676	0.676	8.9551	11.7893	1.5305	1.5187	97.6235
AFI07-32	Hornblende	40.9131	0.8727	11.4373	0.0544	19.7662	0.6631	8.8618	11.6663	1.5049	1.4774	97.2173
AFI07-33	Plagioclase	62.1057	0	23.6349	0	0.1847	0	0	5.1732	8.5902	0.2301	99.9189

ID	Mineral	SiO2	TiO2	Al2O3	Cr2O3	FeO	MnO	MgO	CaO	Na2O	K2O	Total
AFI07-34	Plagioclase	61.4358	0	23.8121	0	0.0724	0.0068	0	5.7306	8.3283	0.1923	99.5784
AFI07-35	Plagioclase	61.266	0	23.3882	0	0.148	0.0017	0	5.4044	8.3194	0.1705	98.6983
AFI07-36	Hornblende	40.323	0.8198	11.6133	0.0567	20.0835	0.6829	8.5696	11.6674	1.4948	1.4619	96.773
AFI07-37	Hornblende	41.0713	0.8522	11.5274	0.0351	19.6513	0.6955	8.7843	11.8298	1.5151	1.4295	97.3916
AFI07-38	Hornblende	41.064	0.6436	11.1124	0.0219	20.4014	0.6982	8.6662	11.9885	1.3253	1.2919	97.2134
AFI07-42	Plagioclase	61.5888	0.029	23.3974	0.0637	0.1506	0.0277	0	5.6131	8.4733	0.1057	99.4493
AFI07-43	Plagioclase	63.281	0.1406	18.1418	0.0593	0.1579	0.0367	0	0	1.0843	14.3652	97.2669
AFI07-44	Hornblende	41.2297	0.9797	11.0544	0.1583	19.2137	0.6861	9.2614	11.6495	1.5105	1.3691	97.1124
AFI07-45	Hornblende	40.9228	0.8895	10.652	0.1298	19.8134	0.7018	9.1273	11.7805	1.4646	1.3162	96.798
AFI07-46	Hornblende	42.9734	0.9338	11.4645	0.1168	18.0156	0.7206	9.3971	11.739	1.3435	1.1992	97.9036
AFI07-47	Hornblende	42.1964	1.0175	11.7591	0.1542	18.0979	0.6167	9.4316	11.8442	1.5369	1.3344	97.989

References

Anderson, J.L., and Smith, D.R. 1995. The effects of temperature and fO2 on the Al-in-hornblende barometer, American Mineralogist, v. 80, p. 549-559.

Colpron, M., Nelson, J.L., Murphy, D.C. 2007. Northern Cordilleran terranes and their interactions through time. GSA Today: v. 17, no. 4/5.pp. 4-10.

Dessureault, Y., Watson, K., Giroux, G., Lee, C., Trimble, R., Barratt, D., Doherty, A., The, H., Stibbard, J. 2006. Technical Report (NI 43-101) for the Minto Project, Hatch, Sherwood Mining Corp. – Minto Project.

Eckstrand, O.R., Sinclair, W.D., Thorpe, R.I. 1995. Geology of Canadian Mineral Deposit Types, Geological Survey of Canada, Geology of Canada, no. 8, Ch. 19, p. 421-446.

Fowler, B. 2007. Interim Management Discussion and Analysis for BCGold Corp. www.sedar.com (System for Electronic Document Analysis and Retrieval for the Canadian Securities Administrators).

Hammarstrom, J.M. and Zen, E., 1986. Aluminum in hornblende: An empirical igneous geobarometer, American Mineralogist, v. 71, p. 1297-1313.

Haselton, H.T., Hovis, G.L., Hemingway, B.S., Robie, R.A. 1983. Calorimetric investigation of the excess entropy of mixing in analbite-sanidine solid solutions: lack of evidence for Na,K short-range order and implications for two-feldspar thermometry, American Mineralogist, v. 68, p. 298-413.

Hawthorne, F. 1981. Crystal chemistry of the amphiboles. Mineralogical Society of America. Reviews in Mineralogy, v. 9A, P. 1-102.

Hollister, L.S., Grissom, G.C., Peters, E.K., Stowell, H.H., and Sisson, V.B., 1987. Confirmation of the empirical correlation of Al in hornblende with pressure of solidification of calc-alkaline plutons, American Mineralogist, v.72, p. 231-239.

Leake, B.E., Woolley, A.R., Arps, C.E.S., Birch, W.D., Gilbert, M.C., Grice, J.D., Hawthorne, F.C., Kato, A., Kisch, H.J., Krivovichev, V.G. and others. 1997. Nomenclature of amphiboles; Report of the Subcommittee on Amphiboles of the International Mineralogical Association, Commission on New Minerals and Mineral Names, American Mineralogist, v. 82, no. 910, p. 1019-1037.

Lowell, J.D., and Guilbert, J.M. 1970, Lateral and Vertical Alteration-Mineralization Zoning in Porphyry Ore Deposits, Economic Geology, v. 65, P. 373-408.

Mortensen, J.K., Emon, K., Johnston, S.T. and Hart, C.J.R., 2000. Age, geochemistry, paleotectonic setting and metallogeny of Late Triassic- Early Jurassic intrusions in the Yukon and eastern Alaska: A preliminary report. In: Yukon Exploration and Geology

Winchester, J.A., and Floyd, P.A. 1977. Geochemical discrimination of different magma series and their differentiation products using immobile elements. Chemical Geology, v. 20, p. 325-343.

Maps taken from http://www.bcgoldcorp.com/main/?carmacksmaps